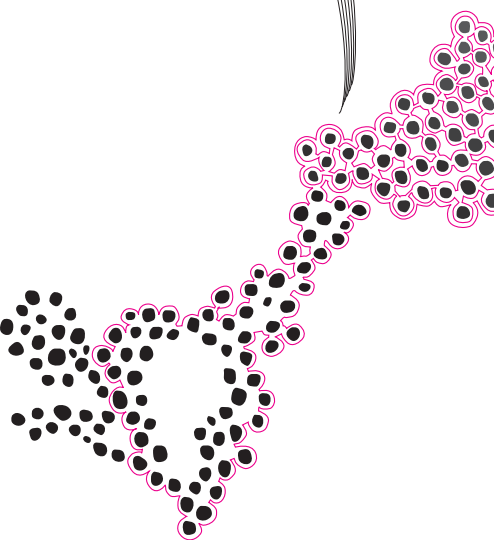BSc Thesis Applied Physics
& Applied Mathematics

Excited-state geometries of small molecules from the GW+Bethe-Salpeter Equation approach

Max Hilt

Supervisors:
dr. L. Leppert
& prof.dr.ir. B.J. Geurts

June, 2023

Department of Applied Physics
Faculty of Science and Technology

Department of Applied Mathematics
Faculty of Electrical Engineering,
Mathematics and Computer Science

UNIVERSITY OF TWENTE.

Preface

I want to thank dr. Linn Leppert and prof.dr.ir. Bernard Geurts for their guidance during my bachelor assignment.

June, 2023

Abstract

In this thesis the GW + Bethe-Salpeter equation (GW + BSE) approach is used to calculate the excited-state geometry of carbon monoxide and thioformaldehyde. The GW method is a many-body perturbation theory which in combination with BSE is able to provide accurate neutral excitation energies in a wide range of systems from molecules to extended solids. Using these neutral excitation energies in combination with ground-state energies obtained using density functional theory allows for the calculation of excited-state energies. A gradient descent algorithm is then applied on the excited-state energies to find the geometry which has the lowest energy, this geometry is the excited-state geometry. Calculating these excited-state geometries with the GW + BSE approach is of importance because essentially all GW + BSE calculations that have been performed to date assume that the excited-state geometry is equal to the ground-state geometry. Other methods have been used to calculate excited-state geometries such as the wavefunction-based equation of motion coupled cluster with single and double excitations (EOM-CCSD) and third order coupled cluster (CC3) methods but these scale with $\mathcal{O}(N^6)$ and $\mathcal{O}(N^7)$ respectively. The GW + BSE approach scales better with $\mathcal{O}(N^4)$ where N denotes the amount of electrons in the system. A systematic benchmark is performed to evaluate how well excited-state geometries from GW+BSE approach agree with reference results from CC3 and EOM-CCSD. In particular, we test the effect of simulation parameters such as the exchange-correlation functional, basis set, and partial self-consistency in the GW approach. This benchmark provides a clear overview of the performance of the GW + BSE approach which can be referenced for future calculations. This comparison is followed by a discussion on the excited-state forces and their potential future applications for molecular dynamics. We conclude that the $GW + BSE$ approach can be used on small molecules to calculate the excited-state geometry with high accuracy whilst being computationally cheaper than the wavefunction based methods.

Keywords: GW, BSE, excited-state geometry, excited-state forces

Contents

1 Introduction

The field of computational physics offers the possibility to predict material properties and investigate interesting material behaviour without having to perform measurements in a lab. In order to perform these calculations a lot of different methods are available. Each method has its own application. When choosing a method its important that the method can accurately determine the desired quantity. Furthermore, it is always desirable to minimize the associated computational costs as much as possible.

In this thesis we are interested in calculating excited-state forces and geometries. This field of physics which is concerned with the behaviour of electrons in atoms molecules and solids is called electronic structure theory. The goal of electronic structure theory is to derive an understanding entirely based upon first principles quantum mechanics. The excited-state forces are necessary for determining how the positions of the atomic nuclei of a molecule change upon excitation of electrons with light. The changes of the positions of the atomic nuclei are then used to go from the ground-state geometry to the excited-state geometry. The transition from the ground-state geometry to the excited-state geometry also induces changes in various photophysical properties which makes calculating excited-state geometries interesting. Current research is also investigating the use of excited states to have efficient exciton transport, this method is called transient delocalization [32]. Furthermore research is also done on directing the path of light-induced electron transfer [13]. These are just two examples of recent research related to excited states.

In this thesis we will be working on electronic excited-state force and geometry calculations within the GW + Bethe-Salpeter equation (GW + BSE) approach which has become one of the most important tools in electronic structure theory. The GW + BSE approach is a Green's function based many-body perturbation theory that allows accurate calculation of charged and neutral excitations in a wide range of systems from molecules to extended solids. In essentially all calculations to date in which the GW+BSE approach is used, it is assumed that the electronic excitations do not affect the positions of the nuclei, so the ground-state geometry is kept even though the system under consideration has been excited. We will go beyond this assumption and use numerical gradients to find the excited-state forces and geometry following the seminal work of Çaylak and Baumeier [8]. We are interested in evaluating how well the excited-state geometries calculated with GW + BSE approach compare with EOM-CCSD and CC3 results. EOM-CCSD and CC3 are both wavefunction-based methods that are commonly used to calculate excited-state forces and geometries and are considered to be very accurate [10, 27]. Investigating the performance of the GW + BSE approach compared with these wavefunction based methods is interesting since the computational costs of the GW + BSE approach scales with $\mathcal{O}(N^4)$[26] where N is the number of electrons in the system. The computational costs of the wavefunction based methods CCSD and CC3 scale with $\mathcal{O}(N^6)$ and $\mathcal{O}(N^7)$ respectively [27, 26].

In order to evaluate the performance of the GW + BSE approach a structured benchmark is performed. The calculations for this benchmark are performed in the open source software MOLGW [4]. The first excited state calculations are done on the carbon monoxide (CO) molecule. This molecule has been chosen because it only has one degree of freedom in its geometry since there is only one bond length that can be changed. Furthermore there are also literature results available on the ground- and excited-state geometry of carbon monoxide which is needed for our benchmark.

The second molecule under consideration is Thioformaldehyde. Thioformaldehyde is already considerably more difficult than carbon monoxide because it has more atoms and thus more degrees of freedom. However, contrary to CO, the first excited state of thioformaldehyde is energetically well-separated from higher-energy excited states. In the case of thioformaldehyde there are four atoms which in total give the molecule six degrees of freedom in the atomic positions. In order to determine the excited-state forces a gradient descent algorithm is applied which is able to find the excited-state geometry. It is able to find this excited-state geometry by taking small steps in the direction opposite of the excited-state forces, which decreases the energy. This procedure is continued until the excited-state forces are lower than a set threshold. The minimum energy of that excited state is then reached, the corresponding geometry is the excited-state geometry.

This thesis will start with three sections that provide an overview of the theory behind the GW + BSE approach used in the simulations. In Section 2, Density Functional Theory is discussed. We then turn to GW in Section 3 and the Bethe-Salpeter Equation approach in Section 4. In Section 5, we discuss our computational methods, simulation settings, coordinates systems and the gradient descent method. After the computational techniques have been discussed, the results are presented in Section 6, starting with the carbon monoxide molecule, which is followed by the results for the thioformaldehyde molecule. In the end we found that with the right simulation settings the GW + BSE approach yields results that are close to the values obtained with wavefunction-based methods. For the excited state of carbon monoxide the excited-state bond length calculated with the best simulation settings has a difference of only $\approx 0.9\%$ with the results of EOM-CCSD. For the excited state of thioformaldehyde there are more degrees of freedom. We investigated four different parameters of the excited state and of these four the largest difference with the CC3 results is just $\approx 0.7\%$. This difference is of the $C-S$ bond length, the other three parameters had even smaller differences. These results show the potential that the GW + BSE approach has, and future research should focus on applying the method on larger molecules and using the forces in molecular dynamics simulations.

2 Density Functional Theory

Density functional theory (DFT) is a much-used method in electronic structure theory. The method was developed in 1964 and 1965 by Hohenberg, Sham and Kohn [23, 20]. The theory is based upon the fact that the observables in Quantum Mechanics can all be determined when the electron density is known, since the wavefunction is a functional of the electron density. In this thesis we use this theory to get an initial estimate of the electron addition and removal energies and to determine the orbitals needed to construct the single-particle Green's function G and the screened Coulomb interaction W for the GW approach. We start our discussion with wavefunction-based quantum mechanics and show why it is not well suited for the many-body problem we are trying to solve. We follow this up with a short introduction to functionals and end the section with DFT focusing on the Hohenberg-Kohn theorem and Kohn Sham equations.

2.1 Wavefunction quantum mechanics

In quantum mechanics the wavefunction $\psi(\mathbf{r})$ is the object which contains all the information about a given system. And the surroundings of the system are all given in the potential of the system $v(\mathbf{r})$ that acts on the electrons [6]. For any system, the potential is given and the wavefunction can be calculated by solving the Schrödinger equation. For a single electron, the Schrödinger equation is given by

$$\left(-\frac{\hbar^2 \nabla^2}{2m} + v(\mathbf{r}) \right) \psi(\mathbf{r}) = E\psi(\mathbf{r}) \tag{1}$$

where $\hbar$ denotes the reduced Planck constant and m the mass which in our case would be the mass of the electron. In case of many-body problems, which is what we are focused on in this thesis, the Schrödinger equation can be extended to a many-body equation. The equation then becomes

$$\left(\sum_i^N \left(-\frac{\hbar^2 \nabla^2}{2m} + v(\mathbf{r}_i) \right) + \sum_{i<j} U(\mathbf{r}_i, \mathbf{r}_j) \right) \psi(\mathbf{r}_1, \mathbf{r}_2, \ldots \mathbf{r}_N) = E\psi(\mathbf{r}_1, \mathbf{r}_2, \ldots \mathbf{r}_N) \tag{2}$$

Here N is the number of electrons in the system and $U(\mathbf{r}_i, \mathbf{r}_j)$ gives the electron-electron interactions in the system. This electron-electron interaction for a Coulomb system is given by

$$\hat{U} = \sum_{i<j} U(\mathbf{r}_i, \mathbf{r}_j) = \sum_{j<i} \frac{q^2}{|\mathbf{r}_i - \mathbf{r}_j|} \tag{3}$$

This operator is not dependent on the particular system under consideration and can thus be applied to all systems, such as atoms, molecules and solids. Furthermore, in the many-body Schrödinger equation, the kinetic energy operator is also used

$$\hat{T} = -\frac{\hbar^2}{2m} \sum_i \nabla_i^2 \tag{4}$$

This operator is not dependent on the system and is always the same. The only thing that changes when one looks at different systems is the potential $v(\mathbf{r}_i)$. Assuming the Born-Oppenheimer approximation, the potential in molecules is given by

$$\hat{V} = \sum_i v(\mathbf{r}_i) = \sum_{i,k} \frac{Q_k q}{|\mathbf{r}_i - \mathbf{R}_k|} \tag{5}$$

Here k extends over all the nuclei in the molecule with charge $Q_k = Z_k e$ and position R_k. Substituting these expressions into the Schrödinger equation gives

$$\left(\hat{T} + \hat{V} + \hat{U} \right) \psi(\mathbf{r}_1, \mathbf{r}_2, \dots \mathbf{r}_N) = E\psi(\mathbf{r}_1, \mathbf{r}_2, \dots, \mathbf{r}_N) \tag{6}$$

Now if we compare the single-body Schrödinger equation (1) with the many-body Schrödinger equation (6) they look almost identical apart from the new $\hat{U}$ term. Even though there is a striking similarity the many-body Schrödinger equation is extremely more difficult to solve because it is a coupled differential equation and the many-body wavefunction is an complicated object whose complexity is exponentially increasing with increasing particle number. So in order to solve the many-body Schrödinger equation we will look at the alternative method, using DFT.

2.2 Electron density quantum mechanics

The procedure to solve quantum mechanics problems using wavefunctions is schematically shown as [6]

$$v(\mathbf{r}) \xrightarrow{\text{Schrödinger Equation}} \psi(\mathbf{r}_1, \mathbf{r}_2, \dots, \mathbf{r}_N) \xrightarrow{<\psi|...|\psi>} \text{Observables} \tag{7}$$

Since we saw in the previous subsection that this method is not convenient to solve the many-body problem we will use another approach. Instead of using the wavefunction we use the electron density as the most important quantity that contains all the information about the system. This approach is an exact method and not an approximation. The electron density is one of the observables in a system and can be calculated with the following formula [6]

$$n(\mathbf{r}) = N \int d^3 r_2 \int d^3 r_3 \cdots \int d^3 r_N \psi^*(\mathbf{r}, \mathbf{r}_2, \dots, \mathbf{r}_N)\psi(\mathbf{r}, \mathbf{r}_2, \dots, \mathbf{r}_N) \tag{8}$$

The goal of DFT is to solve the problem such that the electron density is known and then use this electron density to reconstruct the wavefunction and potential. This is schematically shown as

$$n(\mathbf{r}) \Rightarrow \psi(\mathbf{r}_1, \mathbf{r}_2, \dots, \mathbf{r}_N) \Rightarrow v(\mathbf{r}) \tag{9}$$

Now that the general idea behind DFT is clear we can look into how one actually goes from the electron density to the wavefunction. But before we can state the important Hohenberg-Kohn theorem we first briefly discuss what functionals are.

2.2.1 Functionals

A functional is a mathematical object that maps a function to a number [6]. A simple functional is for example the particle number [6]

$$N[n] = \int d^3 r n(\mathbf{r}) \tag{10}$$

Here $N[n]$ is the functional and the function is $n(\mathbf{r})$.

2.2.2 Hohenberg-Kohn theorem

The Hohenberg-Kohn theorem stands at the core of DFT. This theorem states that the ground-state density can be inverted [6]. So given the ground-state density $n_0(\mathbf{r})$ one can calculate the ground-state wavefunction $\psi_0(\mathbf{r}_1, \mathbf{r}_2, \ldots, \mathbf{r}_N)$. Specifically, the ground-state wavefunction would be a functional of the ground-state density $\psi_0[n_0](\mathbf{r}_1, \mathbf{r}_2, \ldots, \mathbf{r}_N)$. And in turn also the observables would be functionals of the electron density.

This result seems counter intuitive since the ground-state electron density is a function of only $\mathbf{r}$ and the wavefunction is a function of $\mathbf{r}_1, \mathbf{r}_2, \ldots, \mathbf{r}_N$. The crucial thing is that we also know that the ground-state wavefunction must not only reproduce the electron density but must also minimize the energy. This can be written down mathematically as follows [6]

$$E_{v,0} = \min_{\psi \to n_0} \left\langle \psi | \hat{T} + \hat{U} + \hat{V} | \psi \right\rangle \tag{11}$$

Here $E_{v,0}$ denotes the ground-state energy in potential $v(\mathbf{r})$. This equation tells us that we want the wavefunction that reproduces the ground-state electron density and minimizes the energy.

We can also write down the general expression for the total-energy functional [6].

$$E_v[n] = \min_{\psi \to n} \left\langle \psi | \hat{T} + \hat{U} + \hat{V} | \psi \right\rangle = \min_{\psi \to n} \left\langle \psi | \hat{T} + \hat{U} | \psi \right\rangle + \int d^3 r n(\mathbf{r}) v(\mathbf{r}) =: F[n] + V[n] \tag{12}$$

Here, we introduce two new functionals of n. The internal-energy functional is denoted by $F[n]$ and the potential energy functional by $V[n]$. The internal-energy functional is independent of $v(\mathbf{r})$, and is only dependent on the structure of $\hat{U}$ and $\hat{T}$ [6].
Although equation (12) can in theory be used to find the electron density, in practice we will not use it in this form. This is because it is quite a tough numerical problem to find the parameters that minimize the energy, and a good approximation of $F[n]$ is also needed [6].

2.2.3 Kohn Sham equations

There are a lot of different ways DFT can be applied. One of the most often used applications of DFT are the Kohn-Sham equations [6]. The Kohn Sham equations do not work exclusively with the electron density but also make use of single particle orbitals. In order to apply these single particle orbitals we will start by rewriting the kinetic-energy functional. We rewrite the functional in a part that represents the kinetic energy of non-interacting particles $T_s[n]$ and another part representing the remainder $T_c[n]$. An expression of $T_s[n]$ is not known exactly as a functional of n, but it is known as an expression of single particle orbitals $\phi_i(\mathbf{r})$. The expression then becomes [6]

$$T_s[\{\phi_i[n]\}] = -\frac{\hbar^2}{2m} \sum_i^N \int d^3 r \phi_i^*(\mathbf{r}) \nabla^2 \phi_i(\mathbf{r}) \tag{13}$$

Here the notation $T_s[\{\phi_i[n]\}]$ denotes that T_s is an explicit functional of single particle orbitals, and single particle orbitals are functionals of the electron density n. So T_s depends on a complete set of occupied orbitals ϕ_i. With this new expression for $T[n]$ we can once more write down the energy functional

$$E[n] = T_s[\phi_i[n]] + U_H[n] + E_{xc}[n] + V[n] \tag{14}$$

By definition, the exchange correlation energy $E_{xc}[n] = (T[n] - T_s[\{\phi_i[n]\}]) + (U[n] - U_H[n])$. We also introduce the Hartree potential $U_H[n]$ [6] which is given by

$$U_H[n] = \frac{q^2}{2} \int d^3r \int d^3r' \frac{n(\mathbf{r})n(\mathbf{r}')}{|\mathbf{r} - \mathbf{r}'|} \tag{15}$$

Formally, equation (14) is an exact equation, albeit with unknown exchange correlation energy. The Hohenberg Kohn theorem guarantees that it is a functional of the electron density n. Although there is no exact method for finding the exchange correlation energy, several ways of approximating it are known. We will discuss the methods that are used in this thesis in Section 5.2.

The final step to completing DFT is to minimize equation (14). This is however not possible because T_s is a functional of the single particle orbitals ϕ_i and not a functional of the electron density n. The minimization can however be done indirectly by using a scheme that was introduced by Kohn and Sham [23]. The first step is finding the functional derivatives to the electron density [6].

$$0 = \frac{\delta E[n]}{\delta n(\mathbf{r})} = \frac{\delta T_s[n]}{\delta n(\mathbf{r})} + \frac{\delta V[n]}{\delta n(\mathbf{r})} + \frac{\delta U_H[n]}{\delta n(\mathbf{r})} + \frac{\delta E_{xc}[n]}{\delta n(\mathbf{r})} = \frac{\delta T_s[n]}{\delta n(\mathbf{r})} + v(\mathbf{r}) + v_H(\mathbf{r}) + v_{xc}(\mathbf{r}) \tag{16}$$

Here, several familiar important variables are created. The first is $v(\mathbf{r})$, i.e., the external potential. Moreover, $v_H(\mathbf{r})$ is the Hartree potential and $v_{xc}(\mathbf{r})$ the exchange correlation potential. When we look at a system of non-interacting particles moving in a potential $v_s(\mathbf{r})$ the minimization condition is [6]

$$0 = \frac{\delta E}{\delta n(\mathbf{r})} = \frac{\delta T_s[n]}{\delta n(\mathbf{r})} + \frac{\delta V_s[n]}{\delta n(\mathbf{r})} = \frac{\delta T_s[n]}{\delta n(\mathbf{r})} + v_s(\mathbf{r}) \tag{17}$$

Because we have no interactions we do not have the Hartree and exchange correlation terms here. The density solving this equation is $n_s(\mathbf{r})$. Now when comparing the non interacting minimization condition (17) with the minimization condition for the interacting system (16) we see that they have the same solution $n_s(\mathbf{r}) \equiv n(\mathbf{r})$ if $v_s(\mathbf{r})$ is given by

$$v_s(\mathbf{r}) = v(\mathbf{r}) + v_H(\mathbf{r}) + v_{xc}(\mathbf{r}) \tag{18}$$

The electron density of the interacting many-body system in potential $v(\mathbf{r})$ can be calculated by solving the equation for a non-interacting single body system in potential $v_s(\mathbf{r})$. The Schrödinger equation in the auxiliary system becomes

$$\left(-\frac{\hbar^2 \nabla^2}{2m} + v_s(\mathbf{r}) \right) \phi_i(\mathbf{r}) = \epsilon_i \phi_i(\mathbf{r}) \tag{19}$$

This equation yields the orbitals needed to reconstruct $n(\mathbf{r})$, and these are also the orbitals which we have already seen in equation (13) for T_s. So the electron density can be constructed as follows

$$n(\mathbf{r}) \equiv n_s(\mathbf{r}) = \sum_i^\infty f_i |\phi_i(\mathbf{r})|^2 \tag{20}$$

Here f_i denotes the occupation of the i'th orbital. Equation (18) – (20) are the famous Kohn Sham equations which enable the calculation of the electron density without having to minimize the energy as was suggested in equation (12). And with this electron density

in principle all observables of the system can be computed.

One of these observables is the energy of the system. The total energy of the system can be computed using the electron density and the energy functional given in equation (14). This is used to calculate the ground-state energy. For the excitation energies the Kohn-Sham eigenvalues ϵ_i from equation (19) can be used. This might seem odd since the ϵ_i are completely artificial objects and have no physical meaning [6]. However rigorous fundamental considerations and empirical results have shown that they provide a reasonable first approximation to the actual excitation energies [6].

These equations are all implemented in the software MOLGW which is used in this thesis, more information about MOLGW can be found in Section 5.1.

2.2.4 Practical application

When looking through the equations it becomes clear that v_H and v_{xc} both depend on the electron density n. The electron density n in turn is dependent on the single particle orbitals ϕ_i which can be seen in equation (20). And finally the orbitals ϕ_i are again dependent on v_H and v_{xc} which can be seen in equation (18) & (19). So in order to solve the Kohn-Sham equations in practice an iterative process is used. One starts with an initial guess for $n(\mathbf{r})$ then solve the minimization equation to get a new value of the electron density $n_1(\mathbf{r})$. With this new electron density the calculation can be repeated until the electron density converges. This process is called the self-consistency cycle [6].

3 GW method

The GW method was developed by Hedin in 1965 [19] and has become one of the most important tools in electronic structure theory for calculating electron addition and removal energies of a wide range of systems with high accuracy [17]. In its simplest form, the so-called G_0W_0 approach, is used for calculating perturbative corrections to DFT eigenvalues. The aim of electronic structure theory is to derive an understanding entirely based upon first principles of quantum mechanics. In this section we will discuss the G_0W_0 approach that we use in the MOLGW [4] code. We start this section with a derivation relating the G_0W_0 approach to the Kohn-Sham equations. Then we continue with a more in depth explanation of parameters used in the G_0W_0 approach. The section ends with a discussion of the G_nW_n approach, which is a partially self-consistent flavor of GW. In this thesis the GW method will not be used fully self-consistently. For a complete discussion on the GW method and a full derivation of Hedins equations see [17, 19].

3.1 The G_0W_0 approach

In this section, a brief derivation of the G_0W_0 approach is provided, which is instructive for understanding the relationship between GW and DFT. For this derivation we will change to Bra-Ket notation, and start by defining the Kohn-Sham Hamiltonian.

$$H^{KS} = \frac{-\hbar^2}{2m}\nabla^2 + v_{ext} + v_H + v_{xc} \tag{21}$$

Using this Hamiltonian we can rewrite equation (19) in Bra-ket notation,

$$H^{KS}\left|\phi_i^{KS}\right\rangle = \epsilon_i^{KS}\left|\phi_i^{KS}\right\rangle \tag{22}$$

On the other hand, we can write the quasiparticle equation [17] as

$$H^{KS}\left|\phi_i^{GW}\right\rangle - v_{xc}\left|\phi_i^{GW}\right\rangle + \Sigma\left|\phi_i^{GW}\right\rangle = \epsilon_i^{GW}\left|\phi_i^{GW}\right\rangle \tag{23}$$

Σ denotes the self energy which is discussed in the next subsection. ϵ_i^{GW} is the ith excitation energy calculated with the GW method and ϕ_i^{GW} are the GW orbitals. For simplicity we write the self energy as Σ and note that the self energy is non-local, energy dependent and non-Hermitian.

Now we assume that $\phi_i^{GW} \approx \phi_i^{KS}$. This assumption is justified by empirical observations that DFT orbitals are very similar to orbitals from higher-level approaches and their densities can resemble those reconstructed from angle-resolved photo emission spectroscopy for molecules such as pentacene [12]. We assume that this also holds for the molecules we are considering in this thesis. Recombining (22) & (23) with this assumption yields

$$\epsilon_i^{KS}\left|\phi_i^{KS}\right\rangle - v_{xc}\left|\phi_i^{KS}\right\rangle + \Sigma\left|\phi_i^{KS}\right\rangle = \epsilon_i^{GW}\left|\phi_i^{KS}\right\rangle \tag{24}$$

Next we project this on $\langle\phi_i^{KS}|$ which yields

$$\epsilon_i^{GW}\left\langle\phi_i^{KS}|\phi_i^{KS}\right\rangle = \epsilon_i^{KS}\left\langle\phi_i^{KS}|\phi_i^{KS}\right\rangle + \left\langle\phi_i^{KS}\right|\Sigma - v_{xc}\left|\phi_i^{KS}\right\rangle, \tag{25}$$

and, since the KS orbitals are orthonormal

$$\epsilon_i^{GW} = \epsilon_i^{KS} + \left\langle\phi_i^{KS}\right|\Sigma(\epsilon_i^{GW}) - v_{xc}\left|\phi_i^{KS}\right\rangle \tag{26}$$

Here, we have also explicitly written down that the self energy is dependent of ϵ_i^{GW}. So in order to solve equation (26) an iterative procedure must be performed where at each

step the self energy $\Sigma(\epsilon_i^{GW})$ must be recalculated [17]. In practice, this issue is resolved by either finding a graphical solution or, by assuming that the relative difference between ϵ_i^{KS} and ϵ_i^{GW} is sufficiently small, and performing a first order Taylor expansion to evaluate $\Sigma(\epsilon_i^{GW})$ [15, 17]. This avoids having to recalculate the self energy at each iteration until a self consistent value of ϵ_i^{GW} is reached [17].

$$\Sigma(\epsilon_i^{GW}) \approx \Sigma(\epsilon_i^{KS}) + (\epsilon_i^{GW} - \epsilon_i^{KS}) \left.\frac{\partial\Sigma(\epsilon)}{\partial\epsilon}\right|_{\epsilon=\epsilon_i^{KS}} \tag{27}$$

Substituting this Taylor expansion into equation (26) gives as new expression for calculating the GW energies ϵ_i^{GW} [17, 15]

$$\epsilon_i^{GW} = \epsilon_i^{KS} + Z_i \left\langle \phi_i^{KS} | \Sigma(\epsilon_i^{KS}) - v_{xc} | \phi_i^{KS} \right\rangle \tag{28}$$

$$Z_i^{-1} = 1 - \left\langle \phi_i^{KS} \left| \left.\frac{\partial\Sigma(\epsilon)}{\partial\epsilon}\right|_{\epsilon=\epsilon_i^{KS}} \right| \phi_i^{KS} \right\rangle \tag{29}$$

Equation (28) is the final equation that we will apply for finding ϵ_i^{GW}. It also clearly shows that ϵ_i^{GW} is ϵ_i^{KS} with a perturbative correction added [15]. The term Z_i is the renormalization factor [15]. This renormalization factor quantifies how much the spectral weights must be reduced to account for electron-electron interactions [17]. In the case of barely interacting systems the renormalization factor would be almost equal to one [21]. In the next subsection we will discuss the self-energy and the approximation we use to calculate it in more detail.

3.2 Self-energy

As stated earlier the self energy is a non-local, energy dependent and non-Hermitian quantity. In this thesis we are using the GW approximation of the self energy which can be written down as [17, 15]

$$\Sigma = iGW \tag{30}$$

The GW method is named after this approximation for the self energy. G denotes the single-particle Green's function and W the screened Coulomb potential [17]. However in this thesis we will once more approximate this equation for the self energy with the zeroth order of the self energy Σ_0 which can be written down as [17]

$$\Sigma_0 = iG_0W_0 \tag{31}$$

This is the self energy that we will also use when solving equation (28). In the next two subsections the physical interpretation and the zeroth-order approximation of the Green's function and screened Coulomb potential are discussed.

3.2.1 Green's function

The Green's function is an important mathematical tool. In the context of many-body quantum mechanics the definition of the Green's function differs from the common mathematical usage and corresponds to the probability amplitude that an electron is created (annihilated) at location $\mathbf{r}_1$ at time t_1, then propagates through the system for some time

and eventually is annihilated (created) at location $\mathbf{r}_2$ at time t_2. The mathematical expression for this is as follows [17]

$$G(\mathbf{r}_1, t_1, \mathbf{r}_2, t_2) = -i \left\langle \psi_N \left| \hat{T}\{\hat{\psi}(\mathbf{r}_1, t_1)\hat{\psi}^\dagger(\mathbf{r}_2, t_2)\} \right| \psi_N \right\rangle \tag{32}$$

Here ψ_N represents the many-body wavefunction of the system under consideration. Then we have $\hat{\psi}(\mathbf{r}_1, t_1)$ and $\hat{\psi}^\dagger(\mathbf{r}_2, t_2)$ which are the annihilation and creation operator [17] respectively. $\hat{\psi}(\mathbf{r}_1, t_1)$ annihilates an electron at position $\mathbf{r}_1$ at time t_1, and $\hat{\psi}^\dagger(\mathbf{r}_2, t_2)$ creates an electron at position $\mathbf{r}_2$ and time t_2. The final operator is the time ordering operator $\hat{T}$ which makes sure that the annihilation and creation operators are in the correct order.

In this thesis we will be approximating the Green's function with G_0, a zeroth-order approximation which can be calculated from Kohn-Sham orbitals ϕ_i^{KS} and excitation energies ϵ_i^{KS} [17, 15].

$$G_0(\mathbf{r}, \mathbf{r}', \omega) = \sum_m \frac{\phi_i^{KS}(\mathbf{r})\phi_i^{KS*}(\mathbf{r}'))}{\omega - \epsilon_i^{KS} - i\eta sgn(E_f - \epsilon_i^{KS})} \tag{33}$$

Here, η is a convergence parameter, the sign of which is dependent on the energy of the orbital energy that is being added. Finally we have ω which gives the frequency dependency of the Green's function.

3.2.2 Screened Coulomb interaction

The second term of importance is the screened Coulomb potential. The screened Coulomb potential differs from the normal Coulomb potential since it accounts for the screening effects duo to other charges that are in the system. The screening is visually shown in Figure 1. In this figure the annihilation of an electron is shown which creates a hole. After some period the other electrons in the system will concentrate themselves around this new hole. Because of these electrons the hole is screened.
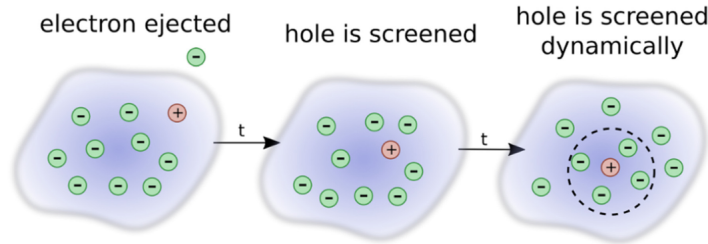

FIGURE 1: Figure showing how a hole is screened, figure from [17].

Because all particles in many-particle systems are screened the concept of quasiparticles is often used [17]. Quasiparticles are not real particles but are rather a different way of looking at a real particle together with the cloud of particles screening it. The addition and removal energies predicted by the GW method are all energies for quasiparticles [17].

The zeroth-order approximation of the screened Coulomb potential $W_0(\omega)$ is written as [17]

$$W_0(\omega) = \epsilon^{-1}(\omega)v - v \tag{34}$$

Here v is the potential of the given system and $\epsilon(\omega)$ is the dielectric function. The dielectric function is then given by [17]

$$\epsilon(\omega) = 1 - v\chi_0(\omega) \tag{35}$$

Here we again see the potential v but now we also have the polarizability $\chi_0(\omega)$. And finally this polarizability on its turn is given by [17]

$$\chi_0(\omega) = \sum_i^{occ} \sum_a^{virt} \left(\frac{\phi_i^{KS*}\phi_a^{KS}\phi_a^{KS*}\phi_i^{KS}}{\omega - \left(\epsilon_a^{KS} - \epsilon_i^{KS}\right) + i\eta} - \frac{\phi_i^{KS*}\phi_a^{KS}\phi_a^{KS*}\phi_i^{KS}}{\omega + \left(\epsilon_a^{KS} - \epsilon_i^{KS}\right) - i\eta} \right) \tag{36}$$

This equation shows that the polarizability can be calculated once the orbitals ϕ_i^{KS} and excitation energies ϵ_i^{KS} from the Kohn-Sham DFT calculation are known. Again just as we have seen for G_0 there is also a convergence parameter η and frequency ω. Since the dielectric function can be calculated with the results of the Kohn-Sham equation so can the dielectric function and the screened Coulomb potential.

3.3 G_nW_n

The G_0W_0 approach we have talked about thus far only adds one correction to the Kohn-Sham eigenvalues ϵ_i^{KS} yielding $\epsilon_i^{G_0W_0}$. As a consequence, its results usually depend on the chosen exchange-correlation functional used to calculate the Kohn-Sham eigensystem. This starting-point dependence can be partially avoided by performing multiple iterations until eigenvalue self-consistency is reached. These GW calculations are denoted as eigenvalue self consistent GW (evGW) [17]. In order to perform such a new iteration the calculation of G_0 and W_0 is repeated now using $\epsilon_i^{G_0W_0}$ instead of ϵ_i^{KS}. This is then used to recalculate the self energy Σ_0 and finally the new energy $\epsilon_i^{G_1W_1}$ is calculated using equation (28) where $e_i^{G_0W_0}$ is replaced with $\epsilon_i^{G_1W_1}$ and ϵ_i^{KS} is replaced with $\epsilon_i^{G_0W_0}$.

It has been shown that evGW improves the HOMO-LUMO gaps however over the entire spectrum it does not yield consistent improvements [17]. Whilst evGW is able to lessen the dependence on the starting point energies ϵ_i^{KS} there will always remain some starting point dependence since we are not updating the orbitals ϕ^{KS}.

In the MOLGW [4] software the amount of performed iterations can be set. To clearly show the amount of iterations we perform we use the notation G_nW_n where $n+1$ denotes the amount of iterations performed.

4 Bethe-Salpeter equation

The Bethe-Salpeter equation is named after Bethe and Salpeter[31]. This equation is used to calculate the energies of neutral excitations, so excitations in which the number of electron in the system stay constant. In this section we once more start with the equation used in the calculations and then explain what all the elements that are used in the equations are. For complete derivations of the approach the interested reader can look at the paper by Bethe and Salpeter [31], the paper of Loos and Blase [25] or the paper by Blase, Duchemin and Jacquemin [3].

4.1 Bethe-Salpeter equation

The BSE can be cast as the following eigenvalue equation [3, 25]

$$\begin{pmatrix} R & C \\ -C^* & -R^* \end{pmatrix} \begin{pmatrix} X_\lambda \\ Y_\lambda \end{pmatrix} = \Omega_\lambda \begin{pmatrix} X_\lambda \\ Y_\lambda \end{pmatrix} \tag{37}$$

This equation consists of several higher dimensional elements and vector elements the most important of which is Ω_λ which contains all the neutral excitation energies that we want to know. In order to get a better idea of what this equation entails we will discuss all other variables in more detail.

The element R is the 'resonant' Hamiltonian block. This resonant Hamiltonian is a 4 dimensional element (ignoring spin) which depends on the indices i, j, a and b. The indices i, j refer to occupied states of the system and the indices a, b refer to unoccupied states of the system. These indices together form two pairs of transition, $i \to a$ and $j \to b$. The resonant Hamiltonian block is given by the following equation [25, 3, 27]

$$R_{ai,bj} = \delta_{a,b}\delta_{i,j}(\epsilon_a^{GW} - \epsilon_i^{GW}) + 2\int\int d\mathbf{r}d\mathbf{r}' \frac{\phi_i^{KS}(\mathbf{r})\phi_a^{KS}(\mathbf{r})\phi_j^{KS}(\mathbf{r}')\phi_b^{KS}(\mathbf{r}')}{|\mathbf{r} - \mathbf{r}'|}$$
$$- \int\int d\mathbf{r}d\mathbf{r}'\phi_i^{KS}(\mathbf{r}')\phi_a^{KS}(\mathbf{r})W(\omega = 0)\phi_j^{KS}(\mathbf{r}')\phi_b^{KS}(\mathbf{r}) \quad (38)$$

The other, 'antiresonant' BSE matrix element reads [25, 3, 27]

$$C_{ai,bj} = 2\int\int d\mathbf{r}d\mathbf{r}' \frac{\phi_i^{KS}(\mathbf{r})\phi_a^{KS}(\mathbf{r})\phi_j^{KS}(\mathbf{r}')\phi_b^{KS}(\mathbf{r}')}{|\mathbf{r} - \mathbf{r}'|} - \int\int d\mathbf{r}d\mathbf{r}'\phi_i^{KS}(\mathbf{r}')\phi_a^{KS}(\mathbf{r})W(\omega = 0)\phi_j^{KS}(\mathbf{r})\phi_b^{KS}(\mathbf{r}')$$
$$(39)$$

Looking at both BSE matrix elements a lot of similarities can be recognized. Both equations contain the screened Coulomb potential $W(\omega = 0)$ which has already been discussed in Section 3.2.2, but is here approximated by neglecting its frequency-dependence. Both screened Coulomb potentials are in integrals where the only difference is that for R ϕ_j^{KS} depends on $\mathbf{r}'$ and ϕ_b^{KS} depends on $\mathbf{r}$ and for C these dependencies are changed so ϕ_j^{KS} depends on $\mathbf{r}$ and ϕ_b^{KS} on $\mathbf{r}'$. Then both elements have the identical bare two-electron integral [27]. Finally, only the resonant Hamiltonian block has the term $\delta_{a,b}\delta_{i,j}(\epsilon_a^{GW} - \epsilon_i^{GW})$ which gives the difference in energy between the occupied state and unoccupied state if $a = b$ and $i = j$.

Then we have X_λ and Y_λ which are the eigenvectors. X_λ^{ia} consist of all the resonant occupied to unoccupied components and Y_λ^{ia} consists of all the non-resonant unoccupied to occupied components [3].

5 Computational methods

5.1 MOLGW

As stated in the introduction the software we use to perform the DFT, GW and BSE simulations is MOLGW [4]. MOLGW is an open source software that can calculate excited electronic states of finite systems using many-body perturbation theory. The calculations were performed on the CCPHead cluster, on the ccp20 and ccp22 partitions [9]. The accompanying self written scripts that were used to automatically run the MOLGW scripts and evaluate the results can be found on GitHub [16].

5.1.1 Simulation settings

In MOLGW there are a lot of simulation settings that can be changed. These simulation settings range from the functional and basis that are used in the simulation to the environment in which the simulations takes place. The functionals and basis will each be discussed in their own separate subsections, see 5.2 & 5.3. In this subsection we will discuss some of the other settings, all settings that are not discussed keep their default value which can be found on the MOLGW website [29].

We start with the settings about the environment in which we place the system we are simulating. Table 1 gives the values of the surroundings during the simulation.

TABLE 1: Values of the environment in which the simulations were performed.

Parameter	Value
Temperature	0 [K]
Magnetization	0 $[\frac{A}{m}]$
Electric field x direction	0 $[\frac{N}{C}]$
Electric field y direction	0 $[\frac{N}{C}]$
Electric field z direction	0 $[\frac{N}{C}]$

These are the default values of the environment which are set by MOLGW. This perfect environment is impossible to create experimentally. Because of this when we evaluate the performance of the GW + BSE approach in the next section, while comparing to experimental results, we use results from wavefunction-based methods as reference.

Apart from the environment there are two other parameters that we have changed. The first parameter is *frozencore* which can be set to 'yes' and 'no'. When *frozencore* is set to 'yes' the core electrons of the atoms are treated as frozen during the calculations, so their distribution is not allowed to respond to the perturbations from the valence electrons. The advantage being that freezing the core electrons is more efficient. During our simulations we set frozencore to 'no' since that should yield slightly more accurate results and the additional computational costs are not a problem since carbon monoxide and thioformaldehyde are both small molecules.

The second parameter is *nstep_gw* which sets the number of GW iterations for eigenvalue self-consistent GW calculations. This parameter is set to ten for the G_9W_9 simulation discussed in Section 6.1.3.

5.2 Functionals

Functionals decide what the expression for $E_{xc}[n]$ becomes which is very important as we saw in sections 2 & 3. There are a lot of different possible functionals to choose from which are categorized in categories such as local, semilocal, gradient-dependent, nonlocal and integral-dependent [6]. In this thesis we will not concern ourselves with all possible functionals but we will focus our attention on three functionals, *BLYP, B3LYP & BHLYP*. Where *BLYP* is a semilocal functional and *B3LYP, BHLYP* are non-local, so-called hybrid functionals [6].

BLYP is a semilocal GGA functional where GGA stands for generalized-gradient approximation [6]. The general expression for the exchange correlation energy for GGA functionals is given in equation (40) [6]. From this expression it becomes clear that the GGA exchange correlation energy is not only dependent on the density of the current position but also on the gradient of the density.

$$E_{xc}^{GGA}[n] = \int d^3r f(n(\mathbf{r}), \nabla n(\mathbf{r})) \tag{40}$$

BLYP is the combination of Becke's exchange functional [1] and Lee's et al. [24] correlation functional. Generally GGAs tend to yield reliable results for the main types of bonding interactions such as covalent, ionic, metallic and hydrogen bridge [6]. The exact expression of the exchange correlation energy can be found by combining the results in the paper of Becke [1] with those of Lee et al. [24]

$$E_{xc} = E_x^{B88} + E_c^{LYP} \tag{41}$$

Then we have the two functionals B3LYP and BHLYP which are both hybrid functionals. Hybrid functionals can be thought of as combinations of the non-local, orbital-dependent Hartree-Fock method and regular density-dependent functionals [28, 2]. The most significant improvement made by hybrid functionals is to the band gaps and excitation energies [28]. Where GGA functionals, such as BLYP, tend to underestimate band gaps and Hartree-Fock tends to overestimates band gaps, hybrids will tend to yield a more accurate prediction of the band gap [28].

The hybrid functionals make use of local density approximation (LDA) functionals, so before we continue we briefly discuss these. For LDA functionals the exchange correlation is calculated by integrating over all space and assuming that that the exchange-correlation energy density at each point is the same as in the homogeneous electron gas [28]. The integral for the exchange correlation energy then looks as follows [6]

$$E_{xc}^{LDA}[n] = \int d^3r e_{xc}^{hom}(n(\mathbf{r})) \tag{42}$$

With this we can now look at the B3LYP functional which is one of the most popular functionals in quantum chemistry [6]. B3LYP uses the Becke B88 exchange functional [28, 1] and the LYP correlation [28, 24] in the following combination [14].

$$E_{xc} = 0.2E_x^{HF} + 0.8E_x^{LDA} + 0.72E_x^{B88} + 0.81E_c^{LYP} + 0.19E_c^{LDA} \tag{43}$$

And then last we have BHLYP which as the H in the name suggests has a 'half-and-half' combination of half LDA exchange and half exact, Hartree Fock like exchange [14]. The BHLYP functional is given in the following equation [14]

$$E_{xc} = \frac{1}{2}E_x^{HF} + \frac{1}{2}E_x^{B88} + E_c^{LYP} \tag{44}$$

Looking at all three functionals a pattern of increasing Hartree Fock exchange can be seen. BLYP has no exact Hartree-Fock like exchange, B3LYP has 20% and BHLYP has 50%.

5.3 Basis sets

When performing numerical simulations the Kohn Sham orbitals must be expressed using a suitable set of basis functions [6]. Finding a suitable basis function is important to have an accurate description of the orbitals. The basis functions that we use in this thesis are *cc-pVDZ, cc-pVTZ, cc-pVQZ & cc-pV5Z.*

The basis functions used in this thesis are all Gaussian basis functions[17]. Gaussian basis functions are by far the most useful for electronic structure calculations of molecules [28] because the product of any two Gaussians is a Gaussian [28]. The number of Gaussians used to describe one orbital are dependent on what type of basis function is used. For *cc-pVDZ* we have a double zeta basis function so two Gaussian are used to describe one orbital. This continues so with *cc-pVTZ* three Gaussians are used, *cc-pVQZ* uses four and finally *cc-pV5Z* uses five Gaussians for each orbital [28].

Hence as the amount of Gaussians used to describe the orbital increases we would expect that the resulting approximation will converge to the true orbital.

5.4 Coordinate systems

In this thesis we use two different coordinate systems which we will briefly discuss.

5.4.1 Nuclear coordinates

Nuclear coordinate are Cartesian coordinates indicating the xyz location of all the atoms in the molecule that is being described. MOLGW requires that the geometry of the molecule is provided in these nuclear coordinates.
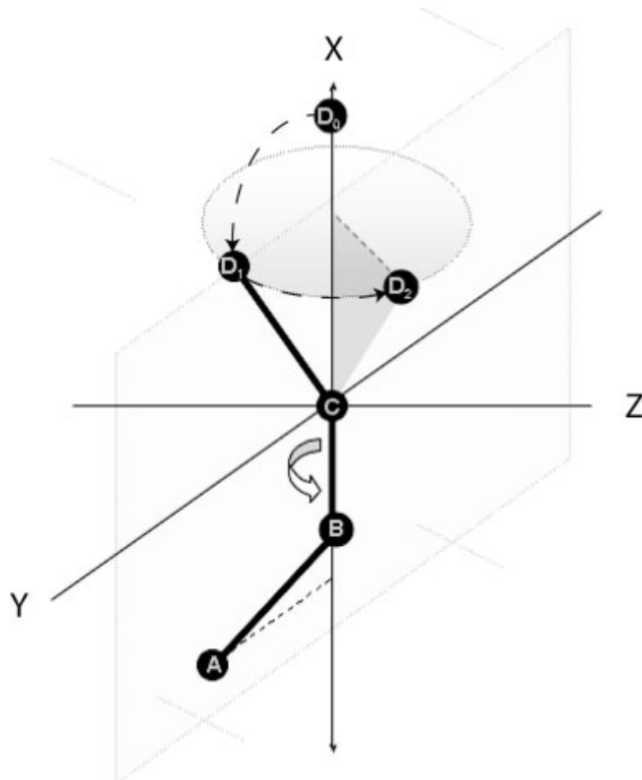
5.4.2 Internal coordinates

FIGURE 2: Illustration of adding new atom to Z matrix, figure from [30].

Although nuclear coordinates are easy to understand they can be difficult if you want to only change one bond length in a molecule, or change one angle in a molecule. For these cases internal coordinates are very useful. Internal coordinates work by choosing one atom as the reference atom and then defining all other atoms using the relative positions they have to other atoms. The internal coordinates are given in the so called Z matrix[34, 33]. In the Z matrix every atom in the system has its separate row, And there are 7 columns. Figure 3 shows an example of such a Z matrix.

Current atom	Distance to atom	Distance [Å]	Third atom for angle	Angle [degrees]	Fourth atom for dihedral angle	Dihedral angle [degrees]
A						
B	A	2				
C	B	1	A	120		
D	C	2	B	120	A	60

FIGURE 3: Example of a Z matrix for the molecule in figure 2. The exact values of the molecule in figure 2 are unknown so they are estimated.

The first column of each row states what the element is that we are currently defining.

Then we get the bond length in column 2 and 3, with column 2 stating with respect to what atom the bond length is being measured and column 3 giving the bond length[34, 33]. Looking at Figure 2 we would then have that the first column is D since in the figure the position of D is being set. Then the second column would state C since the distance is measured to point C and finally the third column would have the bond length, which is estimated to be 2.

Then we get the angle in the system for which we also need column 4 and 5. The angle uses three atoms, which are the atoms in column 1,2 and 4. The fifth column then gives the value of the angle. Again looking at Figure 2 we have that column 4 has B so we are looking at $\angle$DCB, where the order is the same as the order of the columns. Now defining this angle takes us from point D_0 which is just anywhere on the sphere around C to point D_1 which is somewhere on a circle which has the correct distance to point C and the correct angle $\angle$DCB. We estimate that this angle is 120 degrees as can be seen in Figure 3.

Finally there is the dihedral angle which adds column 6 and 7. The dihedral angle needs 4 atoms which are the atoms defined in columns 1, 2, 4 and 6. Then with these four points two groups are made, the first group using the atoms in columns 1, 2 and 4 defines the first plane and the atoms in columns 2, 4 and 6 defines the second plane. The angle these two planes make with each other is the dihedral angle which is given in column 7. Looking one last time at Figure 2 column 6 will have point A in it so we are looking at the angle between the plane DCB and plane CBA, in this thesis I will write the dihedral angle as $\theta(DCB, CBA)$. We estimate that the dihedral angle is 60 degrees as can be seen in Figure 3. This angle aligns with the bond between B and C so the dihedral angle essentially gives how much this bond must be rotated. By setting the dihedral angle we move from point D_1 which was somewhere on the circle to point D_2 which is the final and most importantly unique position for point D.

There are three exceptions to the explanation given above to defining the atoms, and these three exceptions are the first three atoms that are being defined. The first atom only has column one stating what element it is, and no further information in the other columns. The second atom only has the first three columns, so stating what element it is and the distance to the first atom. And the third atom that is defined only has information in the first five columns, so no dihedral angle yet. Because of this the amount of dimensions of internal coordinates are $3N - 6$ (for $N \geq 3$)

Since internal coordinates also posses all the information about the structure of the system they can be mapped into nuclear coordinates and nuclear coordinates can be mapped into internal coordinates. The only difference would be that during the transformation the complete system can have some translation and rotation, but that does not influence the results of our simulations.

5.5 Gradient descent

In order to find the ground and excited-state geometry of the molecules we are simulating we must find the configuration with the minimum energy. If the geometry is still rather simple the minimum can be found by simulating a large range of values and finding the value with the lowest energy. However as the amount of dimensions of the problem increases this approach becomes too computationally expensive. So to avoid having to simulate a huge amount of values we will use the gradient descent algorithm [7, 22].

Gradient descent, also known as steepest descent, is an algorithm designed to find a minima of a given continuous function. In our case this function is the energy surface. The method works by taking small steps in the direction opposite of the gradient of the function that is being minimized. Because the function we are considering is the energy surface this gradient is a excited-state force in our case. If the step size is small enough each step is guaranteed to decrease the value of the function [7]. In this section we will look at how the gradient descent method works and what its limitations are.

5.5.1 Method

The first step to apply the gradient descent algorithm is to calculate numerical derivatives which are needed to construct the gradient. The numerical scheme we use to do this is the central derivative which is given by

$$f'(\rho) = \frac{f(\rho + \Delta\rho) - f(\rho - \Delta\rho)}{2\Delta\rho} \tag{45}$$

Where $\Delta\rho$ is a value that must be chosen. In theory letting $\Delta\rho$ go to zero would yield the exact derivative. However in the case of simulations there are always errors in the values of $f(\rho + \Delta\rho)$ and $f(\rho - \Delta\rho)$ so letting $\Delta\rho$ go to zero will increase the magnitude of these errors, so care must be given to find a value of $\Delta\rho$ that is neither too large nor too small.

In order to construct the gradient of the multi-variable function f under consideration the central derivative must be calculated for all dimensions. Each of these derivatives only varies one variable whilst all other variables remain fixed. In the end adding all these derivatives gives the gradient [7].

Finally once the gradient is known it is multiplied with a factor γ which is the learning rate. The learning rate is a hyper parameter that can be set to ensure that the algorithm takes small steps which prevents it from overshooting the minimum [7, 22]. So having large γ risks overshooting the minimum and setting γ too small will make the steps really small which then requires the algorithm to perform more iterations to reach the minimum, and is thus computationally expensive [22]. Combining all of this yields the following expression for the gradient descent algorithm [7]

$$\mathbf{a}_{n+1} = \mathbf{a}_n - \gamma\nabla F(\mathbf{a}_n) \tag{46}$$

In our application of the gradient descent algorithm the algorithm is terminated once every derivative has a absolute value less than 0.05, this value is determined empirically.

5.5.2 Limitations

Whilst the gradient descent algorithm is useful it does have some limitations [7]. The most important limitation is that the algorithm can also find a local minima instead of the global minimum [7, 22]. If the algorithm finds a local minimum it remains there. This is a problem since the geometry of both the ground and excited state require that the global minimum energy is found. So if the energy surface of carbon monoxide or thioformaldehyde has local minima the minima obtained with the gradient descent algorithm could be completely incorrect.

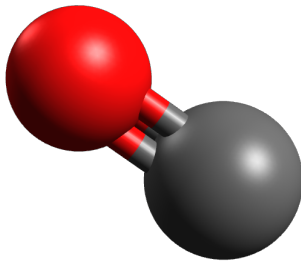# 6 Results & discussion

6.1 Carbon monoxide

FIGURE 4: Illustration of carbon monoxide, figure made with Avogadro[18].

As stated earlier the first molecule under consideration is the carbon monoxide (CO) molecule which can be seen in Figure 4. In the CO molecule there is only one bond length that can be varied which ensures that the problem of finding the ground-state energy and the excited-state energy is only a one dimensional problem. Because this is a one dimensional problem there is no need for a minimum finding algorithm yet. On top of that, this molecule is so small the simulations also do not require a lot of computing time.

We start by looking at the ground state of the CO molecule. The ground-state geometry of the CO molecule is found by minimizing the energy of the ground state. We calculate the energy using DFT which was discussed in Section 2. For these DFT calculations we look at all combinations of functionals *BLYP, B3LYP & BHLYP* and all basis *cc-pVDZ, cc-pVTZ, cc-pVQZ & cc-pV5Z* in order to compare the results.

After the ground state calculations we focus on the first excited state of the CO molecule. The excited-state energies will be calculated using two different methods in order to compare the results. The first method is using DFT + BSE calculations so the excitation energies ϵ_i^{KS} will directly be used in the BSE to get the neutral excitation energies. The second approach is G_0W_0 + BSE, so we take the excitation energies ϵ_i^{KS} and perform one iteration of GW corrections to get the GW excitation energies ϵ_i^{GW}, as was discussed in Section 3, and then use these values in the BSE to get the neutral excitation energies. Once the neutral excitation energies are calculated we add them to the ground-state energy previously calculated using DFT to get the energy of the excited states. In particular we will be looking at the first excited state. All of these calculations will be done for the three functionals *BLYP, B3LYP & BHLYP*, which were discussed in Section 5.2, and the $cc - pV5Z$ basis.

After these simulations have been completed we also look into using several GW iterations instead of one to see the effect this has on the results. We are interested here on how the additional GW iterations change the dependency on the functional we choose for the simulation, since theory suggest that the dependence on the functional should decrease [15].

We end with applying the gradient descent algorithm, discussed in Section 5.5, on the CO molecule. Although the gradient descent algorithm is not needed to find the minimum in the CO molecule it is needed for more complex molecules, such as Thioformaldehyde which is investigated in the next subsection. Hence we apply the gradient descent algorithm on the CO molecule to compare the results of the algorithm with the results from calculating the energy for a whole range of bond lengths to see if the results are the same.

6.1.1 Ground state

As stated we start by looking at the ground state of the CO molecule. In order to optimize the geometry of the CO molecule we only need to find the optimal bond length since this is the only dimension that can be changed. In order to find this minima we perform 400 DFT simulations in MOLGW[4] each with another bond length. The first bond length is 1.000 Å and this is increased in increments of 0.001 Å until the final bond length of 1.400 Å is reached. The resulting graph for one of these simulations can be seen in Figure 5. Then finding the ground-state bond length is as simple as finding the point which achieves the lowest energy.
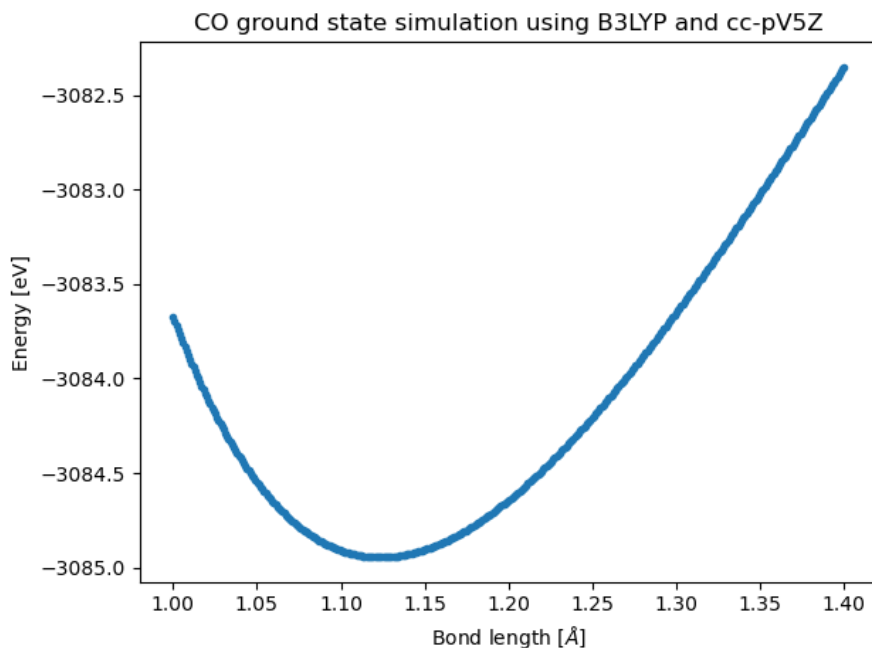
FIGURE 5: Figure showing ground-state energy of the CO molecule as a function of C-O bond length.

This procedure is then repeated for the 12 different combinations of basis and functionals. Figure 6 shows the ground-state bond length calculated using all these different methods.
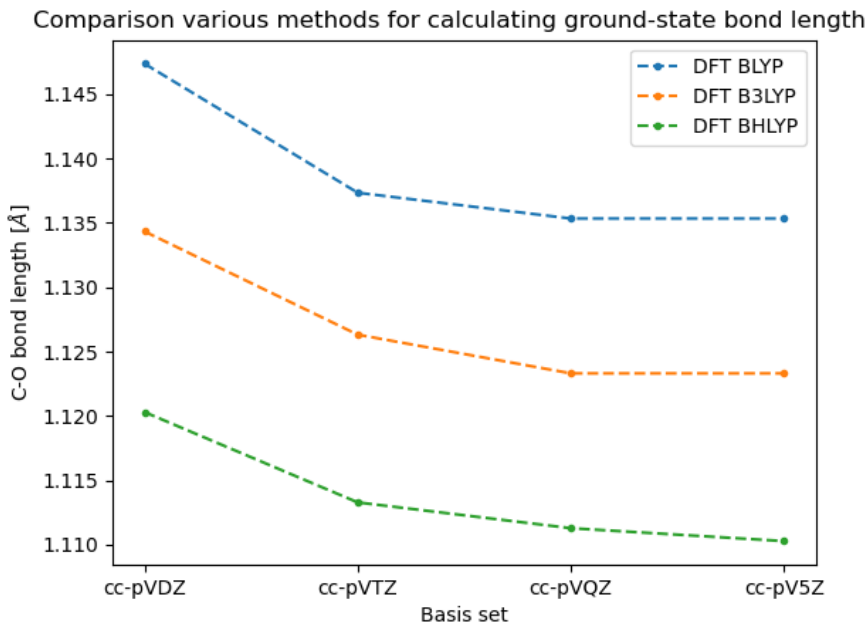
FIGURE 6: Figure showing the calculated ground-state bond length determined for various combinations of functional and basis.

What Figure 6 shows well is that *BLYP, B3LYP & BHLYP* all converge as we go to larger basis sets. This is also what we already expected when we were discussing the basis sets in Section 5.3. Based upon the figure an argument could be made that we are already converged with *cc-pVQZ*. However since the computational costs of the molecules we are considering in the thesis are still low we can use *cc-pV5Z* since the simulations do not take a lot of time. So since *cc-pV5Z* is in theory the most accurate basis set this is the basis set that is used in the remainder of the thesis.

So after setting *cc-pV5Z* as our basis there still are three different values of the C-O bond length, corresponding to the three functionals *BLYP, B3LYP & BHLYP*. Since we want to know how accurate these method are we plot the difference between these methods and the value found in literature for the CC3 method [27]. Looking at this difference gives a good indication on the performance of our method since CC3 is a really accurate wavefunction based method [10]. The reason we prefer the CC3 method over experimental results is that the perfect environment described in 5.1.1 is never achieved during experiment whilst it is achieved in the CC3 simulation.
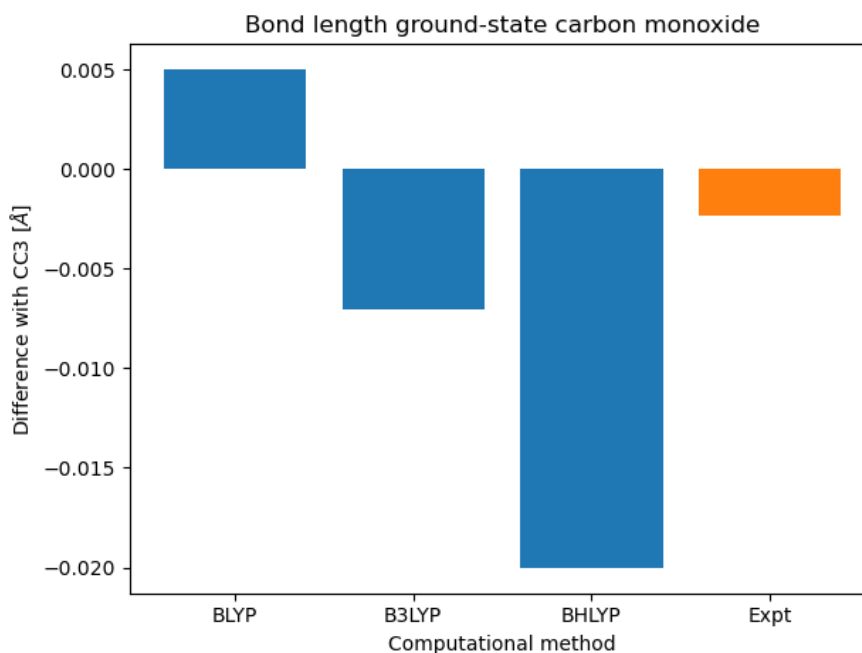
FIGURE 7: Difference ground-state CO bond length of various methods with CO bond length calculated using CC3. CC3 & experimental values from [27].

The numerical values can be found in Table 2 in Section 10.1.1 of the appendix.

As we can see in Figure 7 the functional that seems to yield the best result is BLYP. This result is somewhat surprising since as we discussed in Section 5.2 BLYP is only a semilocal GGA functional whilst both B3LYP and BHLYP are hybrid functionals which we would expect to yield a better result. Nevertheless, the largest error we have is 0.020 Å which is small if we consider that the bond length predicted with CC3 is 1.130 Å. So the largest relative error we have for any of the three functionals is ≈ 1.8%.

6.1.2 Excited state

With the ground-state geometry calculated we can turn our attention to the excited-state geometry. Although looking at the ground state was interesting the main focus we have in this thesis is looking at the excited states using the GW + BSE method. Although the GW + BSE method is our main focus, we also use DFT + BSE since this allows us to compare the results. For both DFT + BSE and GW + BSE 3 simulations are performed, one for each of the three functionals *BLYP, B3LYP & BHLYP* and as stated all simulation have the *cc-pV5Z* basis.

The procedure has not changed much compared with the ground state. We still do 400 simulations each with another bond length. Again starting at 1.000 Å then increasing with increments of 0.001 Å until the final bond length distance of 1.400 Å. The only difference being that the energy of the neutral excitation must be added to the energy of the ground state to get the energy of an excited state. So since we are interested in the first excited state we add the energy of the first excitation to the ground state to get the first excited state. Although this procedure seems simple enough, in practice the excited states can cross each other, this is illustrated in Figure 8.
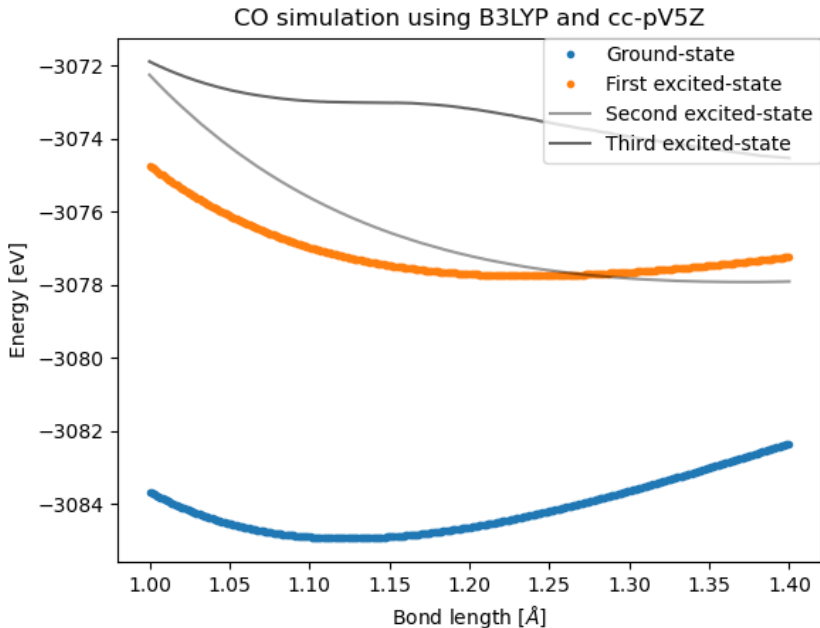

FIGURE 8: Figure showing the ground state with the first three excited states of the carbon monoxide molecule as a function of $C - O$ bond length. Here the results from MOLGW where put through an additional code to correctly handle crossings of excited-state energies.

As can be seen in Figure 8, the first excited state line continues smoothly without any problems when crossing the second excited state line. The problem is that this is not how MOLGW [4] provides the excitation energies. Instead MOLGW [4] will for all 400 different bond lengths label the excitation with the lowest energy as the first excited state. This is not what we physically want since then we are merging two completely different excitations and the minimum of this combination is either the minimum of the first excited state or

the minimum of the second excited state. So the excited-state geometry that is eventually found can then correspond to the wrong excited state.

In the case of the one dimensional CO molecule this problem is relatively easily fixed by looking at when two lines are close and thus identifying where the excited states cross. Then at each intersection the indices of the following points can be corrected such that excited states do not mix. However for molecules with more degrees of freedom, where an algorithm is used to find the minima one should be aware of these crossings. Since identifying these crossings with limited data points is difficult.

In the one dimensional case, I was able to implement a code that is able to correct for these crossings. The code identified possible crossing locations by first going through all the data and looking when the difference in excitation energies is below some threshold. For each of the crossings a whole range of points would be below the threshold. The next step takes this range of points and looks at the point with the smallest difference, this point is taken as the index of the possible crossing. To verify that the lines actually crossed the first derivative would ideally be used, unfortunately due to numerical errors this was quite difficult so the assumption was made that a crossing always happens. This assumption will incorrectly identify two lines that come within the threshold distance of each other without crossing, in practice this was not a problem. After the indices of the crossings were identified the last step was to swap the corresponding columns in the matrix starting at the row of the crossing index until the last index. With these corrections searching for the minimum value is again simply looking for the lowest value. Doing so for the first excited state yielded the following results
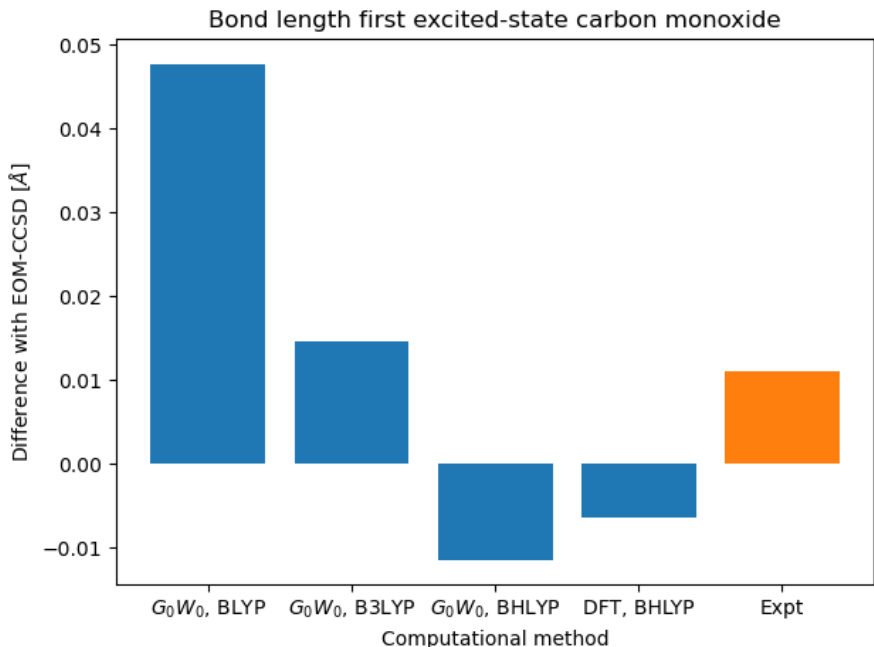

FIGURE 9: Bar graph showing the difference in bond length of the first excited state of CO with EOM-CCSD for various methods. EOM-CCSD & experimental value from [8].

The numerical values can be found in Table 3 & 4 in Section 10.1.1 of the appendix.

The first thing noticeable when looking at Figure 9 is that there is no result for DFT with the *BLYP* and *B3LYP* functionals. This is because for both of these functionals the BSE step in the MOLGW simulation resulted in an error for the Cholesky decomposition of the BSE matrix. A more detailed investigation of this problem would have required to search the source code of MOLGW and was beyond the scope of this thesis.

What is remarkable is that DFT BHLYP seems to match the best with the value of EOM-CCSD found in the paper from Caylak and Baumeier [8] since we would expect GW to have a better result. Since DFT did not even converge with both other functionals we expect that this is just a coincidence but it is interesting to look into further.

Furthermore comparing Figure 9 with Figure 7 we notice that the *BLYP* functional seem to be the worst for calculating the bond length of the first excited state whilst it was the best for calculating the bond length of the ground state. At the same time the *BHLYP* functional seems to have gone from the worst functional to the best functional for calculating the bond length. So there is not one functional that is best suited for both the ground state and excited state simulation.

The relative error of *BLYP* is now $\approx 3.9\%$, and all other functionals have lower errors. So even for the worst functional we are still quite close to the theoretical value of the EOM-CCSD approach.

6.1.3 Performing multiple GW iterations

In Section 3 we discussed the GW method and showed that the GW method can be performed with several iterations. Up to this point we have only focused our attention on G_0W_0 but performing more GW iterations can improve the results obtained so to see this we now perform ten iterations so the approach we use is $G_9W_9 +$ BSE. The following graph shows the resulting bond length together with the bond length obtained using the $G_0W_0 +$ BSE approach and the experimental value.
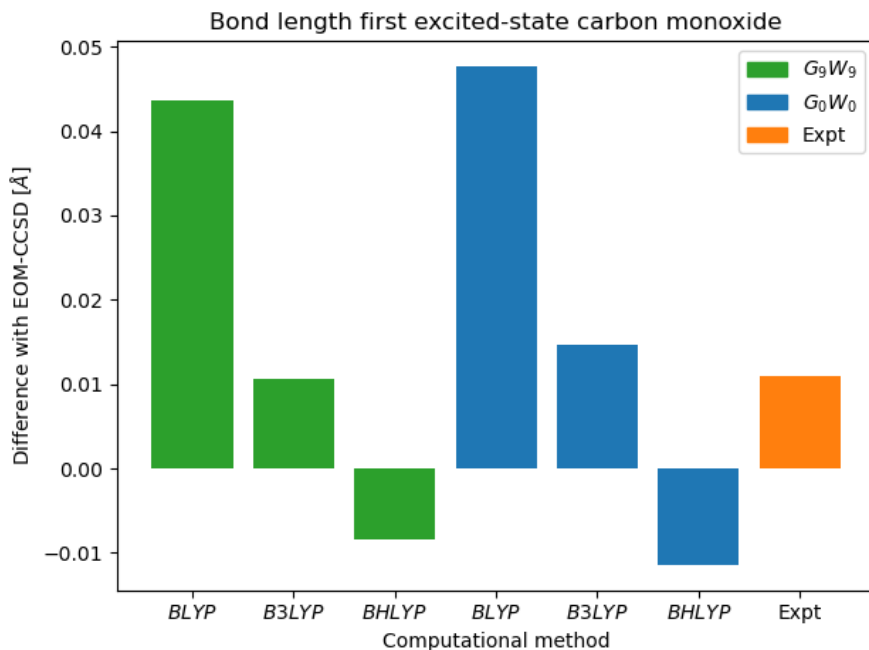
FIGURE 10: Bar graph comparing G_nW_n, G_0W_0 and experiment results. The values are the differences of these methods with the EOM-CCSD results from [8].

Looking at the results in Figure 10 we can see that performing more GW iterations does not seem to have a significant effect on the results. We see that the value of G_9W_9, *BLYP* is slightly lower than G_0W_0 *BLYP* and the value of G_9W_9 *BHLYP* is slightly higher than the value of G_0W_0 *BHLYP* so performing more iterations lets the values of the three functionals converge slightly. However the effect is rather minor.

6.1.4 Gradient descent

Before we apply the gradient descent methods on Thioformaldehyde in the next section we apply it on the CO molecule to evaluate its performance. If the gradient descent algorithm yields the same results as performing 400 separate simulations then we can be more confident in the approach. Since B3LYP was quite good in both determining the bond length of the ground state and the first excited state we will use that functional.
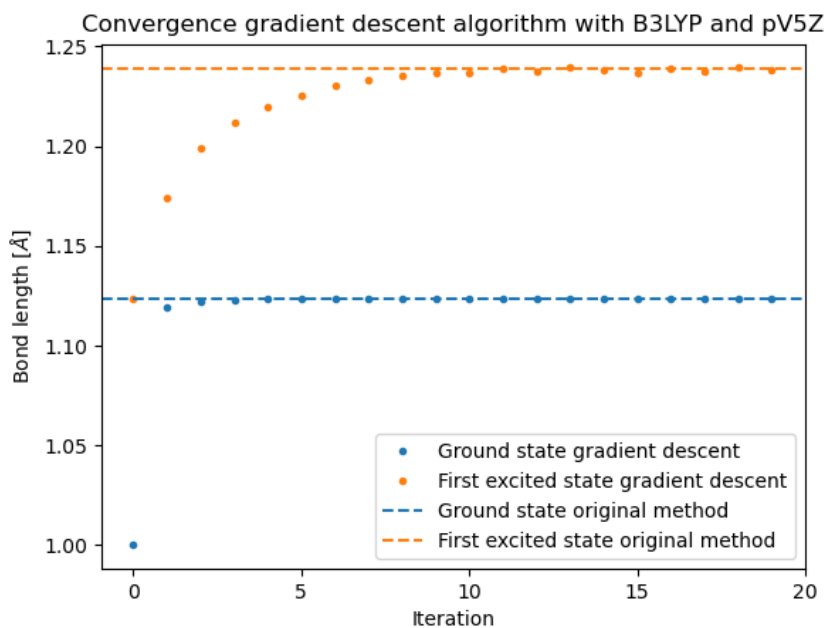
FIGURE 11: Comparing the new gradient descent method with the old method of performing 400 simulations for finding the ground-state and first excited-state bond length.

Figure 11 shows the result of using the gradient descent algorithm on the CO molecule. And it can clearly be seen that the algorithm converges towards the values found in Sections 6.1.1 & 6.1.2. For these simulations the learning rate was set to 0.005 and the distance between grid points $\Delta\rho$ was set to 0.010. Based on this application on the CO molecule we are certain that the gradient descent algorithm is able to locate local minima properly.

6.2 Thioformaldehyde
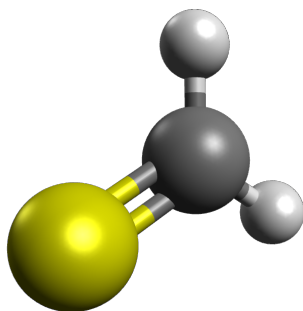
FIGURE 12: Illustration of thioformaldehyde, figure made with Avogadro[18].

The second molecule we are looking at in this thesis is Thioformaldehyde which can be seen in Figure 12. Thioformaldehyde consists of four atoms, two hydrogen, one carbon and one sulfur atom which together give thioformaldehyde six degrees of freedom. This atom is specifically chosen because the excitation energies do not intersect each other which makes it possible to find the minima with the gradient descent algorithm.

We start this section with looking at the ground state of thioformaldehyde and finding the ground-state geometry. This is then also done for the first exited state of thioformaldehyde. Both the ground-state and first excited-state geometry will then be compared with results from literature to see how well the G_0W_0 + BSE approach performs.

We end the section by looking at the six dimensional energy surface in more detail. We will do so by varying two degrees of freedom and keeping the other degrees of freedom fixed. The resulting energy surfaces can be looked at to inspect if there are any local minima on which the gradient descent algorithm can get stuck, yielding an incorrect result. When looking at the energy surface of the first excited state we will also plot the energy surface of the second excited state to verify that we have no crossings since that can also cause problems for the employed gradient descent algorithm.
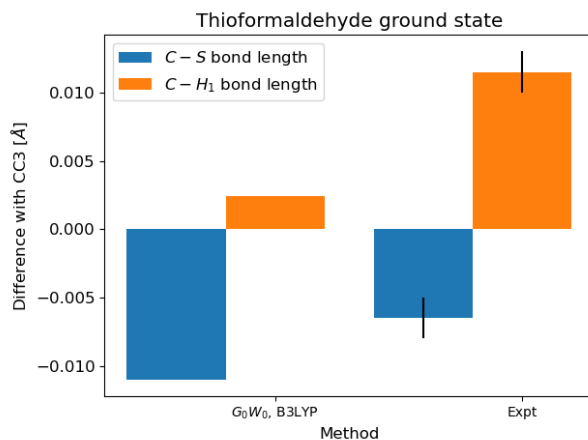
6.2.1 Ground state

FIGURE 13: Difference ground-state geometry with CC3 results. CC3 and Experiment results are from [11].
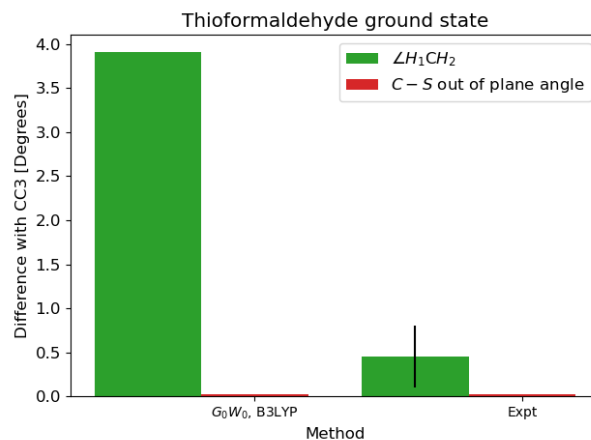

FIGURE 14: Difference ground-state geometry with CC3 results. CC3 and Experiment results are from [11].

The exact values can be found in Table 9 in Section 10.1.2 of the appendix.

Figure 13 & 14 show the difference with CC3 of our results and the experimental results. The results for the $C - S$ and $C - H_1$ bond length are almost the same as CC3 results with relative errors of $\approx -0.7\%$ and $\approx 0.2\%$ respectively. The result for $\angle$ HCH does differ quite a lot unfortunately and finally the $C - S$ out of plane angle is identical with the CC3 result.
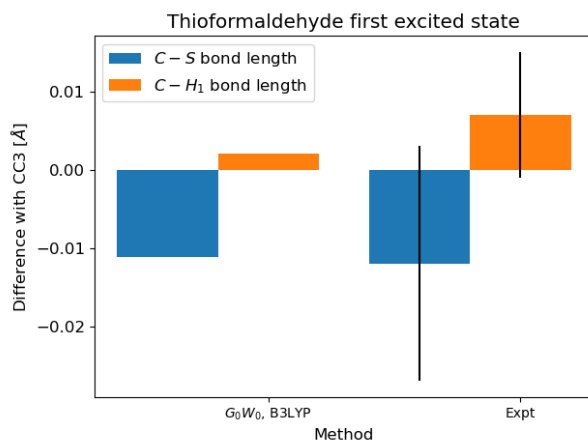
6.2.2 Excited state

FIGURE 15: Difference first excited-state geometry with CC3 results. CC3 and Experiment results are from [5].
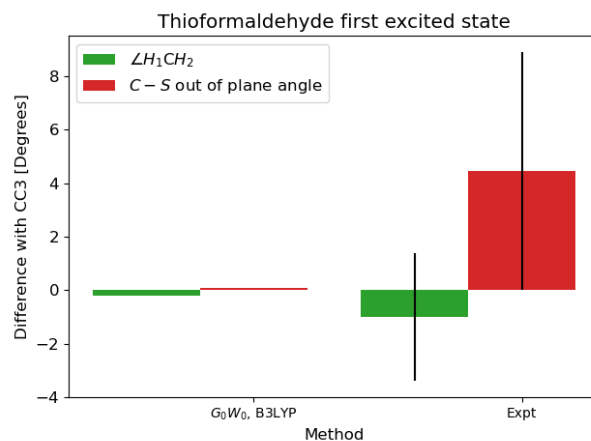

FIGURE 16: Difference first excited-state geometry with CC3 results. CC3 and Experiment results are from [5].

The exact values can be found in Table 10 in Section 10.1.2 of the appendix.

In the case of the excited state we have that the $C - S$ bond length again almost the same as the CC3 bond length having a relative error of $\approx -0.6\%$. The $C - H_1$ bond length is really close to the CC3 value having a relative error of just 0.2%. Finally $\angle$ HCH is almost a perfect match and again the CS out of plane angle is identical with the result from CC3.

6.2.3 Verification of convergence

As discussed in Section 5.5 the gradient descent algorithm is not guaranteed to find the global minimum. We will now analyse the energy surface around the minima found by the gradient descent algorithm to determine if the gradient descent algorithm was able to find the global minima of thioformaldehyde.

The procedure we perform to do this is the following, first we take the minimum found by the gradient descent algorithm. Then we fix four of the six dimensions we have and vary the other two dimensions around the equilibrium value. Finally we plot the resulting three dimensional plane to see if there are any local minima. This procedure is then repeated four times where each time different combinations of variables are varied until every one of the six variables is in at least one of resulting plots.

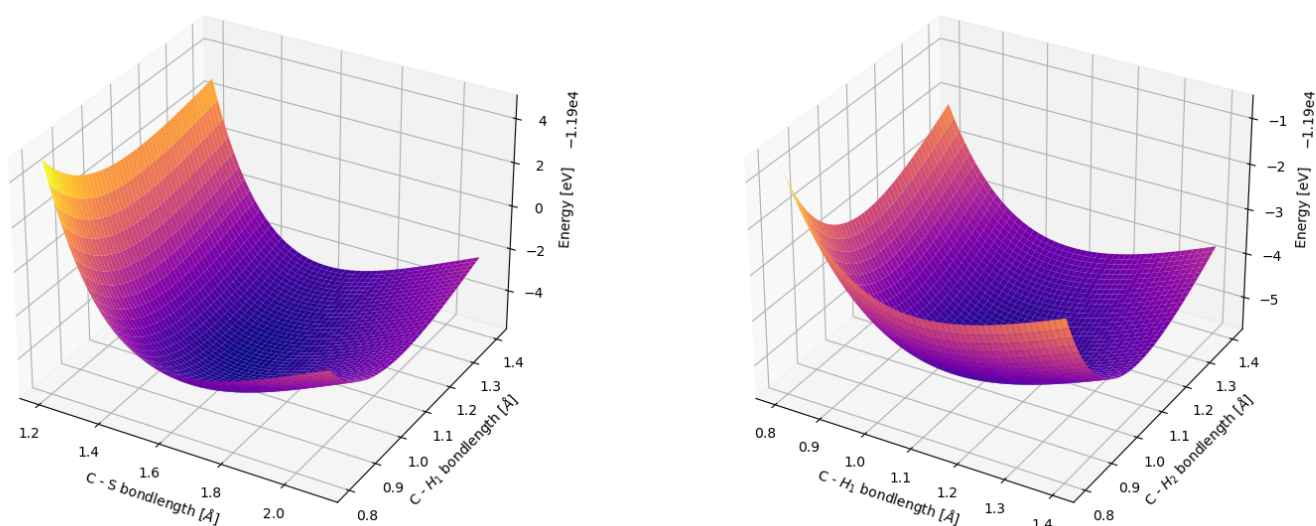We start by looking at the ground state.

FIGURE 17: Plots showing the energy if two of the parameters are varied whilst the other four are kept at equilibrium value of the ground state.

Figure 17 shows the first two plots. The plot on the left varies the bond length between C and S and the bond length between C and H_1. This figure is smooth and does not show and local minima. Then looking at the figure on the right which varies the bond lengths $C - H_1$ and $C - H_2$ we again see a smooth surface and no local minima. So thus far we have not found anything which could cause issues with the gradient descent algorithm we are employing.
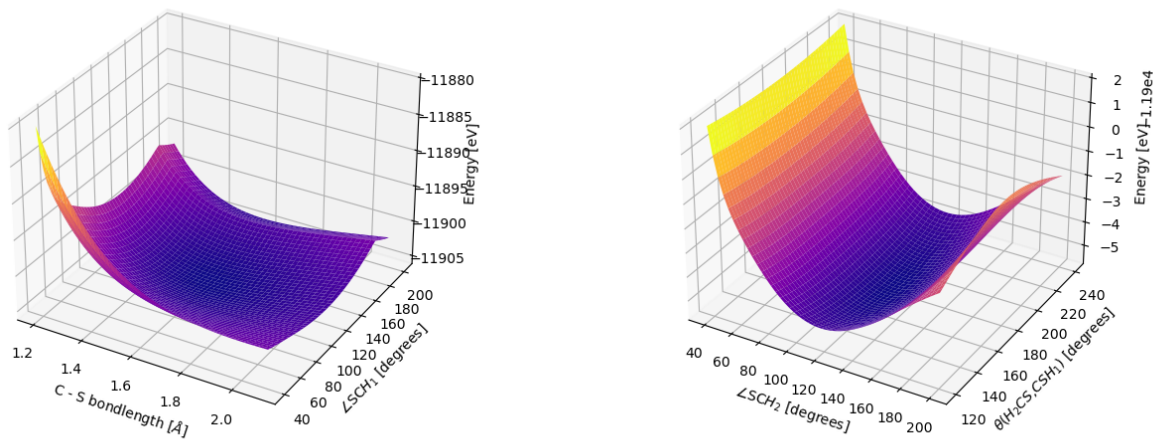
FIGURE 18: Plots showing the energy if two of the parameters are varied whilst the other four are kept at equilibrium value of the ground state.

Now we look at Figure 18 starting with the figure on the right which shows the $\angle SCH_2$ angle and $\theta(H_2CS, CSH_1)$ dihedral angle. This plot is again smooth with no local minima. However the plot on the left does have local minima. One can see that if the $\angle SCH_1$ angle is increased above approximately 160 degrees the gradient descent algorithm will not find our equilibrium value of 120 degrees. However since this would require the gradient descent algorithm to first increase in energy to move from 120 to 160 degrees we can be certain that the gradient descent algorithm is not ending up there. So again no local minima in which the algorithm could have run.

Excited state

Now for the excited state we will not only be looking at the energy surface of the first excited state, but the energy surface of the second excited state is also shown. So we will see if the first excited state has any local minima and also determine if the first and second excited state have any intersections, since that can also cause the gradient descent algorithm to find the incorrect minimum.
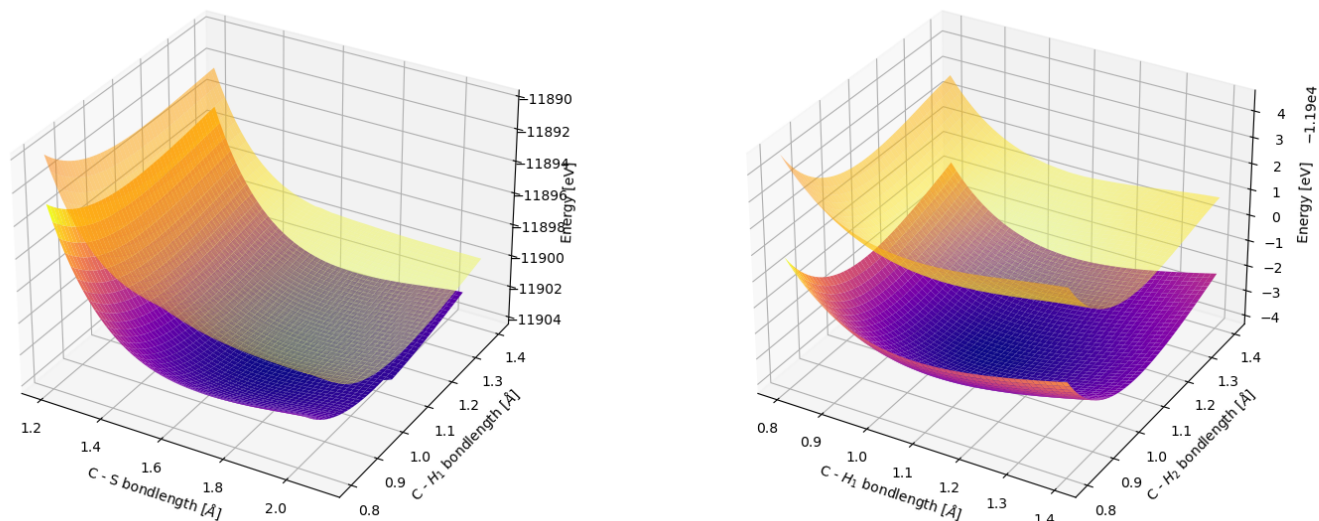

FIGURE 19: Two plots showing the energy surface of the first excited state in dark blue (Bottom) and second excited state in bright yellow (Top).

Figure 19 varies the same parameters as Figure 17, and for the first excited-state energy surface we still have no local minima on either surface. Looking at the second excited-state energy surface we see that they do not have any intersections.
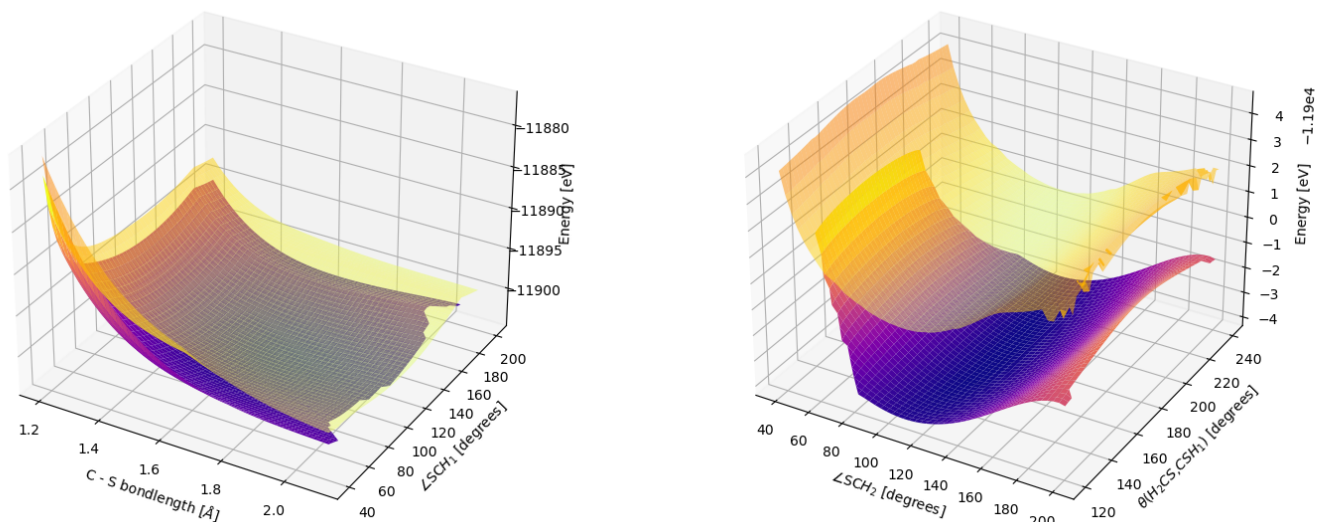
FIGURE 20: Two plots showing the energy surface of the first excited state in dark blue (Bottom) and second excited state in bright yellow (Top).

And finally we have Figure 20 which varies the same parameters as Figure 18. And again the first excited state looks almost identical to the ground state. We still have the same local minima if the $\angle SCH_1$ angle becomes too big. But since our ground state equilibrium has the $\angle SCH_1 = 120$ we know that is not a problem since the gradient descent algorithm would first have to increase in energy which it won't. Furthermore looking at both the first and second excited state we again see no intersections.

Based upon these figures we can be confident that the gradient descent algorithm converged to the global minimum in the ground state and first excited state.

6.3 Excited-state forces

Excited-state forces are forces that the atoms in a molecule experience when an electronic excitation occurs. Although there are a lot of references discussing excited-state geometries, excited-state forces do not share the same kind of popularity. This is rather unfortunate since knowing the excited-state forces is a first step to having molecular dynamics simulations of excitations. Since we do find them important we will look at the excited-state forces that occur when carbon monoxide and thioformaldehyde are excited from the ground state to the first excited state.
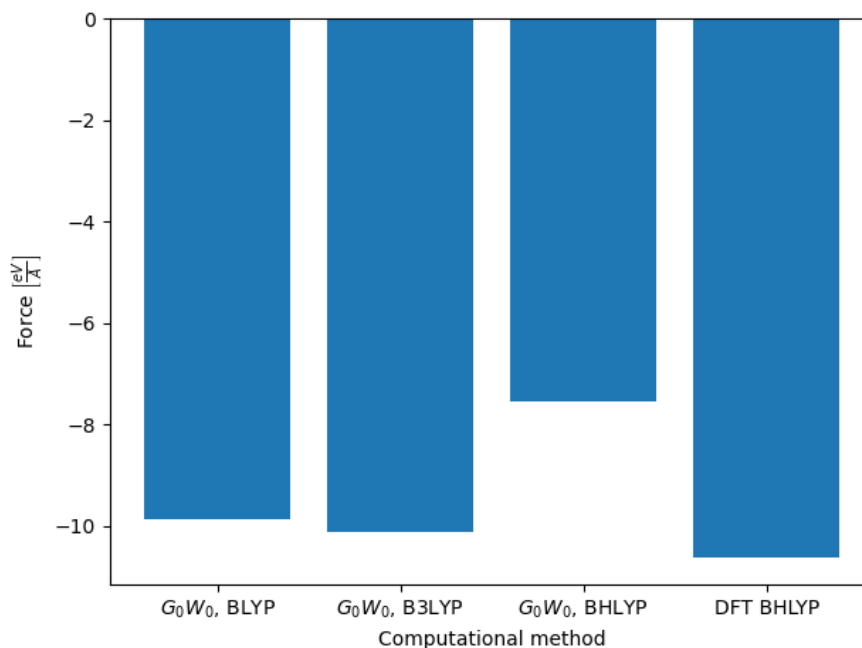
6.3.1 Carbon monoxide

FIGURE 21: Excited-state forces of first excited state carbon monoxide.

The exact values can be found in Table 6 & 4 in Section 10.1.1 of the appendix.

Figure 21 shows the excited-state forces for carbon monoxide. Unfortunately no literature results are available to compare to so all we have are the simulations we performed ourselves. Looking at these simulations we see that they all match rather well except $BHLYP$ which differs quite significantly. This is not surprising since $BHLYP$ predicted the smallest $C - O$ bond length and this small decrease already causes the gradient on the first excited state to be significantly higher, this can be seen when looking at Figure 8.

So the dependence of the excited-state force on the ground-state geometry is large. Hence a functional which works well for determining the ground-state geometry is very important. It may even be best to use two different functionals, one functional that suits the ground state well such as $BLYP$ for carbon monoxide and another functional that suits the excited state well such as $BHLYP$.
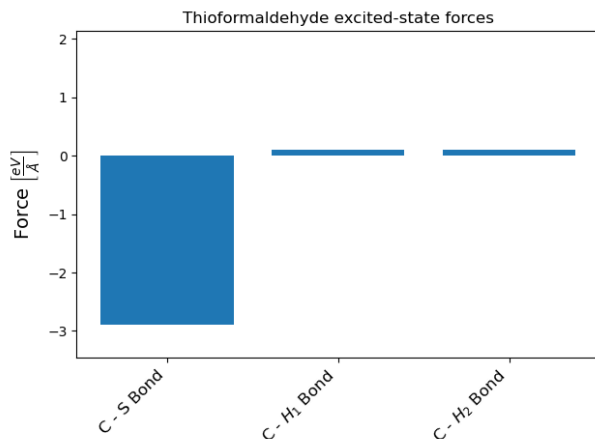
6.3.2 Thioformaldehyde

FIGURE 22: The excited-state forces that thioformaldehyde experienced due to a change in bond length during the electronic excitation from ground state to first excited state. Calculations performed with G_0W_0 + BSE and *B3LYP*.
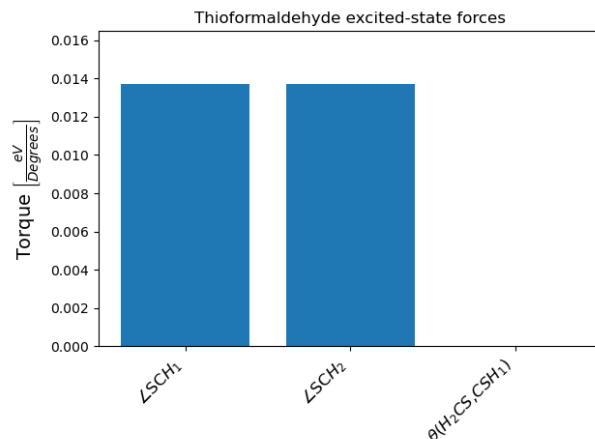

FIGURE 23: The excited-state forces that thioformaldehyde experienced due to a change in angle during the electronic excitation from ground state to first excited state. Calculations performed with G_0W_0 + BSE and *B3LYP*.

The exact values can be found in Table 11 in Section 10.1.2 of the appendix.

Figure 22 & 23 give the excited-state forces that Thioformaldehyde experienced during the electronic excitation. From these figures we can see that the biggest force occurred on the $C - S$ bond, this is not surprising since the $C - S$ bond also experiences the largest change during the excitation which can be seen in Table 9 & 10.

7   Conclusion

In this thesis we performed a systematic benchmark to evaluate the performance of the GW + BSE approach to find the excited-state forces and geometry. This benchmark was performed by scrutinizing several parameters and investigating the effect they have on the results.

Our results for the ground-state and excited-state geometry of carbon monoxide calculated with G_0W_0 + BSE approach show a good match with results from theory. In the case of the ground-state bond length the *BLYP* functional only has a 0.005 Å difference with an CC3 calculation. And the *BHLYP* functional which has the biggest difference with CC3 still only has a difference of 0.020 Å of the ground-state bond length which is a relative error of just 1.8%. When looking at the excited-state geometry of carbon monoxide the *BHLYP* functional achieves a difference with EOM-CCSD of just 0.01 Å and the *BLYP* functional which has the biggest difference with theory only differs 0.05 Å.

Our benchmark also showed that the chosen functional has a large influence on the obtained geometry. This is unfortunate since it will not be clear when new calculations are performed which functional is most accurate for the system under consideration. One method of mitigating this functional dependence is performing several GW iterations. However in the case of the carbon monoxide molecule performing G_9W_9 + BSE simulations yielded only a slight decrease in the difference of the three different functionals that were considered.

The combination of the G_0W_0 + BSE approach with the gradient descent algorithm applied on thioformaldehyde was also in good agreement with results from theory. For both the ground state and first excited state the bond lengths are within 1% of the CC3 result and the $C - S$ out of plane angle are identical with the CC3 result. Only in the ground state the $\angle H_1CH_2$ differs significantly from the CC3 result, having a difference of 3.9 degrees. Finally we presented the excited-state forces that were numerically determined using the G_0W_0 + BSE approach. These forces again showed a significant dependence on the chosen functional.

In conclusion we were able to use the GW + BSE approach on small molecules to calculate the excited-state geometry with high accuracy. Furthermore we were also able to numerically determine the excited-state forces.

8 Future research

In this thesis we showed that the GW + BSE approach can be used to accurately predict the excited-state geometry of small molecules. For future researchers interested in using the GW + BSE approach to calculate excited-state geometries we have several suggestions.

First it would be interesting to also apply the method on larger molecules. Since the GW + BSE approach scales with $\mathcal{O}(N^4)$ [26] it should be able to simulate large molecules that are computationally too expensive for wavefunction based methods such as CC3 which scales with $\mathcal{O}(N^7)$ [26].

Furthermore to get a better understanding of excitation events one could perform molecular dynamics simulations with the excited-state forces calculated with the GW + BSE approach. Molecular dynamics simulations are already performed in current research, for example the research on transient delocalization used molecular dynamics [32]. So a possible new computationally more efficient molecular dynamics simulation will be valuable in current research.

Finally more research could be done on how to handle complex energy surfaces. Difficult phenomena such as local minima and intersections of excited-state energy surfaces can make it difficult to find the global minima. One could look at incorporating a more robust minima finding algorithm that replaces the gradient descent algorithm used in this thesis.

9 References

References

[1] A. D. Becke. "Density-functional exchange-energy approximation with correct asymptotic behavior". In: *Physical Review A* 38.6 (Sept. 1988). Publisher: American Physical Society, pp. 3098–3100. DOI: 10.1103/PhysRevA.38.3098. URL: https://link.aps.org/doi/10.1103/PhysRevA.38.3098 (visited on 06/11/2023).

[2] Axel D. Becke. "A new mixing of Hartree–Fock and local density-functional theories". en. In: *The Journal of Chemical Physics* 98.2 (Jan. 1993), pp. 1372–1377. ISSN: 0021-9606, 1089-7690. DOI: 10.1063/1.464304. URL: https://pubs.aip.org/aip/jcp/article/98/2/1372-1377/821432 (visited on 06/12/2023).

[3] Xavier Blase, Ivan Duchemin, and Denis Jacquemin. "The Bethe–Salpeter equation in chemistry: relations with TD-DFT, applications and challenges". en. In: *Chemical Society Reviews* 47.3 (Feb. 2018). Publisher: The Royal Society of Chemistry, pp. 1022–1043. ISSN: 1460-4744. DOI: 10.1039/C7CS00049A. URL: https://pubs.rsc.org/en/content/articlelanding/2018/cs/c7cs00049a (visited on 04/25/2023).

[4] Fabien Bruneval et al. "molgw 1: Many-body perturbation theory software for atoms, molecules, and clusters". en. In: *Computer Physics Communications* 208 (Nov. 2016), pp. 149–161. ISSN: 0010-4655. DOI: 10.1016/j.cpc.2016.06.019. URL: https://www.sciencedirect.com/science/article/pii/S0010465516301990 (visited on 05/11/2023).

[5] Šimon Budzák, Giovanni Scalmani, and Denis Jacquemin. "Accurate Excited-State Geometries: A CASPT2 and Coupled-Cluster Reference Database for Small Molecules". en. In: *Journal of Chemical Theory and Computation* 13.12 (Dec. 2017), pp. 6237–6252. ISSN: 1549-9618, 1549-9626. DOI: 10.1021/acs.jctc.7b00921. URL: https://pubs.acs.org/doi/10.1021/acs.jctc.7b00921 (visited on 06/09/2023).

[6] Klaus Capelle. "A bird's-eye view of density-functional theory". In: *arXiv: Materials Science* (Nov. 2002). ARXIV_ID: cond-mat/0211443 MAG ID: 2951313239 S2ID: dd93b926eb3bab45f7e6efbc5e01748d104da4b8. DOI: 10.1590/s0103-97332006000700035.

[7] M Augustine Cauchy. "Me´thode ge´ne´rale pour la re´solution des syste'mes d'e´quations simultane´es". en. In: ().

[8] Onur Çaylak and Björn Baumeier. "Excited-State Geometry Optimization of Small Molecules with Many-Body Green's Functions Theory". eng. In: *Journal of Chemical Theory and Computation* 17.2 (Feb. 2021), pp. 879–888. ISSN: 1549-9626. DOI: 10.1021/acs.jctc.0c01099.

[9] *CCPHead Cluster*. URL: https://www.utwente.nl/en/tnw/ccp/infrastructure/ccphead/.

[10] Rachel Crespo-Otero and Mario Barbatti. "Recent Advances and Perspectives on Nonadiabatic Mixed Quantum–Classical Dynamics". en. In: *Chemical Reviews* 118.15 (Aug. 2018), pp. 7026–7068. ISSN: 0009-2665, 1520-6890. DOI: 10.1021/acs.chemrev.7b00577. URL: https://pubs.acs.org/doi/10.1021/acs.chemrev.7b00577 (visited on 06/18/2023).

[11] Monika Dash et al. "Excited States with Selected Configuration Interaction-Quantum Monte Carlo: Chemically Accurate Excitation Energies and Geometries". In: *Journal of Chemical Theory and Computation* 15.9 (Sept. 2019). Publisher: American Chemical Society, pp. 4896–4906. ISSN: 1549-9618. DOI: 10.1021/acs.jctc.9b00476. URL: https://doi.org/10.1021/acs.jctc.9b00476 (visited on 06/09/2023).

[12] M. Dauth et al. "Orbital Density Reconstruction for Molecules". en. In: *Physical Review Letters* 107.19 (Nov. 2011), p. 193002. ISSN: 0031-9007, 1079-7114. DOI: 10.1103/PhysRevLett.107.193002. URL: https://link.aps.org/doi/10.1103/PhysRevLett.107.193002 (visited on 06/01/2023).

[13] Milan Delor et al. "Directing the path of light-induced electron transfer at a molecular fork using vibrational excitation". en. In: *Nature Chemistry* 9.11 (Nov. 2017). Number: 11 Publisher: Nature Publishing Group, pp. 1099–1104. ISSN: 1755-4349. DOI: 10.1038/nchem.2793. URL: https://www.nature.com/articles/nchem.2793 (visited on 06/29/2023).

[14] *Density Functional Theory*. URL: https://www.cup.uni-muenchen.de/ch/compchem/energy/dft1.html.

[15] M. Giantomassi et al. "Electronic properties of interfaces and defects from many-body perturbation theory: Recent developments and applications". en. In: *physica status solidi (b)* 248.2 (2011). _eprint: https://onlinelibrary.wiley.com/doi/pdf/10.1002/pssb.201046094, pp. 275–289. ISSN: 1521-3951. DOI: 10.1002/pssb.201046094. URL: https://onlinelibrary.wiley.com/doi/abs/10.1002/pssb.201046094 (visited on 06/20/2023).

[16] *Github code*. URL: https://github.com/Max-Hilt/Bachelor-project.git.

[17] Dorothea Golze, Marc Dvorak, and Patrick Rinke. "The GW Compendium: A Practical Guide to Theoretical Photoemission Spectroscopy." In: *Frontiers in chemistry* 7 (July 2019). MAG ID: 2962009064, pp. 377–377. DOI: 10.3389/fchem.2019.00377.

[18] Marcus D. Hanwell et al. "Avogadro: an advanced semantic chemical editor, visualization, and analysis platform". In: *Journal of Cheminformatics* 4.1 (Aug. 2012), p. 17. ISSN: 1758-2946. DOI: 10.1186/1758-2946-4-17. URL: https://doi.org/10.1186/1758-2946-4-17 (visited on 06/09/2023).

[19] Lars Hedin. "NEW METHOD FOR CALCULATING THE ONE-PARTICLE GREEN'S FUNCTION WITH APPLICATION TO THE ELECTRON-GAS PROBLEM". In: *Physical Review* 139 (Aug. 1965). MAG ID: 2011327487, pp. 796–823. DOI: 10.1103/physrev.139.a796.

[20] P. Hohenberg and W. Kohn. "Inhomogeneous Electron Gas". In: *Physical Review* 136.3B (Nov. 1964). Publisher: American Physical Society, B864–B871. DOI: 10.1103/PhysRev.136.B864. URL: https://link.aps.org/doi/10.1103/PhysRev.136.B864 (visited on 05/22/2023).

[21] Mark S. Hybertsen and Steven G. Louie. "Electron correlation in semiconductors and insulators: Band gaps and quasiparticle energies." In: *Physical Review B* 34.8 (Oct. 1986). MAG ID: 2014094922, pp. 5390–5413. DOI: 10.1103/physrevb.34.5390.

[22] Kadir Kiran. "A Benchmark Study on Steepest Descent and Conjugate Gradient Methods-Line Search Conditions Combinations in Unconstrained Optimization". en. In: *Croatian operational research review* 13.1 (July 2022), pp. 77–97. ISSN: 18489931. DOI: 10.17535/crorr.2022.0006. URL: https://hrcak.srce.hr/280265 (visited on 06/29/2023).

[23] W. Kohn and L. J. Sham. "Self-Consistent Equations Including Exchange and Correlation Effects". In: *Physical Review* 140.4A (Nov. 1965). Publisher: American Physical Society, A1133–A1138. DOI: 10.1103/PhysRev.140.A1133. URL: https://link.aps.org/doi/10.1103/PhysRev.140.A1133 (visited on 05/22/2023).

[24] Chengteh Lee, Weitao Yang, and Robert G. Parr. "Development of the Colle-Salvetti correlation-energy formula into a functional of the electron density". In: *Physical Review B* 37.2 (Jan. 1988). Publisher: American Physical Society, pp. 785–789. DOI: 10.1103/PhysRevB.37.785. URL: https://link.aps.org/doi/10.1103/PhysRevB.37.785 (visited on 06/11/2023).

[25] Pierre-François Loos and Xavier Blase. "Dynamical correction to the Bethe–Salpeter equation beyond the plasmon-pole approximation". en. In: *The Journal of Chemical Physics* 153.11 (Sept. 2020), p. 114120. ISSN: 0021-9606, 1089-7690. DOI: 10.1063/5.0023168. URL: https://pubs.aip.org/aip/jcp/article/199606 (visited on 06/21/2023).

[26] Pierre-François Loos, Anthony Scemama, and Denis Jacquemin. "The Quest for Highly Accurate Excitation Energies: A Computational Perspective". In: *The Journal of Physical Chemistry Letters* 11.6 (Mar. 2020). Publisher: American Chemical Society, pp. 2374–2383. DOI: 10.1021/acs.jpclett.0c00014. URL: https://doi.org/10.1021/acs.jpclett.0c00014 (visited on 06/28/2023).

[27] Pierre-François Loos et al. "Pros and Cons of the Bethe–Salpeter Formalism for Ground-State Energies". en. In: *The Journal of Physical Chemistry Letters* 11.9 (May 2020), pp. 3536–3545. ISSN: 1948-7185, 1948-7185. DOI: 10.1021/acs.jpclett.0c00460. URL: https://pubs.acs.org/doi/10.1021/acs.jpclett.0c00460 (visited on 06/28/2023).

[28] Richard M. Martin. *Electronic Structure Basic Theory and Practical Methods*. 2nd ed. University Printing House, Cambridge CB2 8BS, United Kingdom: Cambridge university press, 2020.

[29] MOLGW. URL: http://www.molgw.org/.

[30] Jerod Parsons et al. "Practical conversion from torsion space to Cartesian space for in silico protein synthesis". en. In: *Journal of Computational Chemistry* 26.10 (2005). _eprint: https://onlinelibrary.wiley.com/doi/pdf/10.1002/jcc.20237, pp. 1063–1068. ISSN: 1096-987X. DOI: 10.1002/jcc.20237. URL: https://onlinelibrary.wiley.com/doi/abs/10.1002/jcc.20237 (visited on 06/01/2023).

[31] E. E. Salpeter and H. A. Bethe. "A Relativistic Equation for Bound-State Problems". In: *Physical Review* 84.6 (Dec. 1951). Publisher: American Physical Society, pp. 1232–1242. DOI: 10.1103/PhysRev.84.1232. URL: https://link.aps.org/doi/10.1103/PhysRev.84.1232 (visited on 05/11/2023).

[32] Alexander J. Sneyd, David Beljonne, and Akshay Rao. "A New Frontier in Exciton Transport: Transient Delocalization". en. In: *The Journal of Physical Chemistry Letters* 13.29 (July 2022), pp. 6820–6830. ISSN: 1948-7185, 1948-7185. DOI: 10.1021/acs.jpclett.2c01133. URL: https://pubs.acs.org/doi/10.1021/acs.jpclett.2c01133 (visited on 06/29/2023).

[33] Dr. Williams. *The Z-matrix in Computational Chemistry 5381 2019 L07*. Youtube. URL: https://www.youtube.com/watch?v=_4Px1tPy8GY.

[34] *Z-matrix Coordinates*. URL: https://manual.q-chem.com/4.3/sect0015.html.

10   Appendix

10.1   Tables

10.1.1   Tables carbon monoxide

TABLE 2: Bond length ground state carbon monoxide

Functional & Basis	Bond length [Å]
BLYP, cc-pVDZ	1.147368421
BLYP, cc-pVTZ	1.137343358
BLYP, cc-pVQZ	1.135338346
BLYP, cc-pV5Z	1.135338346
B3LYP, cc-PVDZ	1.13433584
B3LYP, cc-PVTZ	1.126315789
B3LYP, cc-PVQZ	1.123308271
B3LYP, cc-PV5Z	1.123308271
BHLYP, cc-PVDZ	1.120300752
BHLYP, cc-PVTZ	1.113283208
BHLYP, cc-PVQZ	1.111278195
BHLYP, cc-PV5Z	1.110275689

TABLE 3: Bond length first excited state of carbon monoxide using DFT + BSE

Functional & Basis	Bond length [Å]
BLYP, cc-pVDZ	x
BLYP, cc-pVTZ	x
BLYP, cc-pVQZ	x
BLYP, cc-pV5Z	x
B3LYP, cc-PVDZ	x
B3LYP, cc-PVTZ	x
B3LYP, cc-PVQZ	x
B3LYP, cc-PV5Z	x
BHLYP, cc-PVDZ	x
BHLYP, cc-PVTZ	1.224561
BHLYP, cc-PVQZ	1.219549
BHLYP, cc-PV5Z	1.217544

TABLE 4: Bond length first excited state carbon monoxide using G_0W_0 + BSE

Functional & Basis	Bond length [Å]
BLYP, cc-pVDZ	1.295739348
BLYP, cc-pVTZ	1.282706767
BLYP, cc-pVQZ	1.274686717
BLYP, cc-pV5Z	1.271679198
B3LYP, cc-PVDZ	1.268671679
B3LYP, cc-PVTZ	1.24962406
B3LYP, cc-PVQZ	1.24160401
B3LYP, cc-PV5Z	1.238596491
BHLYP, cc-PVDZ	1.240601504
BHLYP, cc-PVTZ	1.22556391
BHLYP, cc-PVQZ	1.215538847
BHLYP, cc-PV5Z	1.212531328

TABLE 5: Bond length first excited state carbon monoxide using G_9W_9 + BSE

Functional & Basis	Bond length [Å]
BLYP, cc-pV5Z	1.267669173
B3LYP, cc-pV5Z	1.234586466
BHLYP, cc-pV5Z	1.215538847

TABLE 6: Excited-state forces of first excited state carbon monoxide using DFT + BSE

Functional & Basis	Force $\left[\frac{eV}{\text{Å}}\right]$
BLYP, cc-pVDZ	x
BLYP, cc-pVTZ	x
BLYP, cc-pVQZ	x
BLYP, cc-pV5Z	x
B3LYP, cc-PVDZ	x
B3LYP, cc-PVTZ	x
B3LYP, cc-PVQZ	x
B3LYP, cc-PV5Z	x
BHLYP, cc-PVDZ	x
BHLYP, cc-PVTZ	-10.87647636
BHLYP, cc-PVQZ	-10.65331357
BHLYP, cc-PV5Z	-10.62593279

TABLE 7: Excited-state forces first excited state CO using G_0W_0 + BSE

Functional & Basis	Force $\left[\frac{eV}{\text{Å}}\right]$
BLYP, cc-pVDZ	-7.102188628
BLYP, cc-pVTZ	-11.03559966
BLYP, cc-pVQZ	-10.75629756
BLYP, cc-pV5Z	-9.875095388
B3LYP, cc-PVDZ	-11.77027197
B3LYP, cc-PVTZ	-11.9143381
B3LYP, cc-PVQZ	-11.23211713
B3LYP, cc-PV5Z	-10.11359903
BHLYP, cc-PVDZ	-11.57088808
BHLYP, cc-PVTZ	-6.676587398
BHLYP, cc-PVQZ	-10.60954825
BHLYP, cc-PV5Z	-7.540031877

TABLE 8: Excited-state forces of first excited state carbon monoxide using G_9W_9 + BSE

Functional & Basis	Force $\left[\frac{eV}{\text{Å}}\right]$
BLYP, cc-pV5Z	-9.77085165
B3LYP, cc-pV5Z	-9.674998284
BHLYP, cc-pV5Z	-11.43240655

10.1.2 Tables thioformaldehyde

TABLE 9: Ground-state geometry thioformaldehyde using cc-pV5Z, B3LYP, G_0W_0 + BSE

	Magnitude
$C - S$	1.60797 [Å]
$C - H_1$	1.08541 [Å]
$\angle$ HCH	120.00745826655526 [deg]
Out of plane angle $C - S$	0.0 [deg]

TABLE 10: Excited-state geometry thioformaldehyde using cc-pV5Z, B3LYP, G_0W_0 + BSE

	Magnitude
$C - S$	1.69790 [Å]
$C - H_1$	1.08012 [Å]
$\angle$ HCH	120.00710298234027 [deg]
Out of plane angle $C - S$	0.0 [deg]

TABLE 11: Excited-state forces of first excited state thioformaldehyde using cc-pV5Z, B3LYP, G_0W_0 + BSE

Parameter	Excited-state force
$C - S$ bond length	-2.88429096 $\left[\frac{eV}{\text{Å}}\right]$
$C - H_1$ bond length	0.11073035 $\left[\frac{eV}{\text{Å}}\right]$
$C - H_2$ bond length	0.11073435 $\left[\frac{eV}{\text{Å}}\right]$
$\angle$SCH1	0.01372497 $\left[\frac{eV}{\deg}\right]$
$\angle$SCH2	0.01372597 $\left[\frac{eV}{\deg}\right]$
$\theta(H_2CS, CSH_1)$	0 $\left[\frac{eV}{\deg}\right]$